

AD 731 226

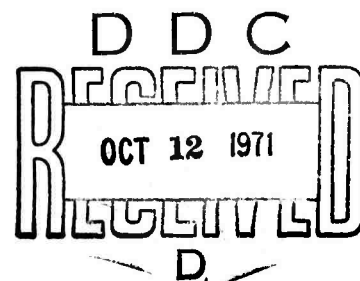
# DAMAGE THRESHOLD STUDIES IN LASER CRYSTALS: SELF-FOCUSING EXPERIMENTS AND ELECTRON HEATING THEORY

By  
Concetto R. Giuliano  
Donald F. DuBois  
Gerald R. Rickel

HUGHES RESEARCH LABORATORIES  
HUGHES AIRCRAFT COMPANY  
3011 Malibu Canyon Road  
Malibu, California 90265

Contract NO. F19628-69-C-0277  
Project NO. 8693

SEMIANNUAL REPORT NO. 4  
JULY 1971



APPROVED FOR PUBLIC RELEASE; DISTRIBUTION UNLIMITED.

Contract Monitor: Erlan S. Bliss, Capt., USAF  
OPTICAL PHYSICS LABORATORY

Sponsored by  
Advanced Research Projects Agency  
ARPA Order No. 1434  
Monitored by  
AIR FORCE CAMBRIDGE RESEARCH LABORATORIES  
AIR FORCE SYSTEMS COMMAND  
UNITED STATES AIR FORCE  
BEDFORD, MASSACHUSETTS 01730

Reproduced by  
NATIONAL TECHNICAL  
INFORMATION SERVICE  
Springfield, Va. 22151

67

## DOCUMENT CONTROL DATA - R&amp;D

(Security classification of title, body of abstract and indexing annotation must be entered when the overall report is classified)

1. ORIGINATING ACTIVITY (Corporate author) Hughes Research Laboratories 3011 Malibu Canyon Road Malibu, California 90265		2a. REPORT SECURITY CLASSIFICATION Unclassified	
		2b. GROUP	
3. REPORT TITLE DAMAGE THRESHOLD STUDIES IN LASER CRYSTALS: SELF-FOCUSING EXPERIMENTS AND ELECTRON HEATING THEORY			
4. DESCRIPTIVE NOTES (Type of report and inclusive dates) Scientific. Interim.			
5. AUTHOR(S) (First name, middle initial, last name) Concetto R. Giuliano, Donald F. DuBois, and Gerald R. Rickel			
6. REPORT DATE July 1971		7a. TOTAL NO. OF PAGES 62	7b. NO. OF REFS 17
8a. CONTRACT OR GRANT NO. F19628-69-C-0277		9a. ORIGINATOR'S REPORT NUMBER(S) Semi-Annual Report No. 4	
b. PROJECT, TASK, WORK UNIT NOS. 8693		9b. OTHER REPORT NO(S) (Any other numbers that may be assigned this report) AFCRL-71 0398	
c. DOD ELEMENT 61101D			
d. DOD SUBELEMENT			
10. DISTRIBUTION STATEMENT Approved for public release; distribution unlimited.			
11. SUPPLEMENTARY NOTES Tech, Other		12. SPONSORING MILITARY ACTIVITY AF Cambridge Research Labs (OP) L.G. Hanscom Field Bedford Massachusetts 01730	
13. ABSTRACT In this report details of the temporal development of damage tracks are presented and discussed in terms of a self-focusing theory. The results of a number of streak camera photographs show that the damage track grows in a way which depends on the temporal behavior of the leading edge of the incident pulse. This work constitutes the first direct evidence for a moving self-focus in solids. A comparison with self-focusing theory is given and the importance of electrostriction is made evident. Damage thresholds in sapphire for lenses of different focal length are presented and compared with the results obtained for ruby in the last report. Also in this report damage with cylindrical lenses is discussed. It was not possible for us to generate damage using cylindrical lenses even though the power density was greater than ten times the power density required to reach damage threshold with a spherical lens giving the same focal spot area. This result suggests that self-focusing is sensitive to beam shape and may point to a possible solution to the problem of damage in high power laser devices. Also in this report an observation of rings in the beam profile of the focused laser beam is presented. The phenomenon which appears at points beyond the beam waist is a property of the ruby laser or possibly a combination of the laser and the lenses. This behavior could well be a general property of "single mode" solid state lasers. Further theoretical effort has been devoted to the problem of heating of electrons in polar crystals by intense optical fields. A kinetic equation has been developed which appears to offer a basis for settling the question of electron heating.			

UNCLASSIFIED

Security Classification

14. KEY WORDS	LINK A		LINK B		LINK C	
	ROLE	WT	ROLE	WT	ROLE	WT
Bulk Damage Damage Thresholds Lasers Ruby Sapphire Streak Camera Experiments Self-Focusing Moving Self Focus Cylindrical Lenses Avalanche Theory Gaussian Beams Beam Profile Measurements Beam Distortion						

UNCLASSIFIED

Security Classification

Program Code No. . . . . 9D10  
 Effective Date of Contract . . . . 21 May 1969  
 Contract Expiration Date . . . . 15 July 1972  
 Principal Investigator . . . . . Concetto R. Giuliano  
 and Phone No. . . . . 213 456-6411 Ext. 208  
 Project Scientist or . . . . . Erlan S. Bliss, Capt. USAF  
 Engineer and Phone No. . . . . 617 861-2600

ACCESSION for	
CESTI	WRITE SECTION <input checked="" type="checkbox"/>
DDC	BUFF SECTION <input type="checkbox"/>
MAN. CED.	<input type="checkbox"/>
JUSTIFICATION	
BY	
DISTRIBUTION/AVAILABILITY CODES	
DIST.	AVAIL. and/or SPECIAL
A	

*Qualified requestors may obtain additional copies from the  
 Defense Documentation Center. All others should apply to  
 the National Technical Information Service.*

AFCRL-71 0398

DAMAGE THRESHOLD STUDIES IN LASER CRYSTALS:  
SELF-FOCUSING EXPERIMENTS AND ELECTRON HEATING THEORY

*by*

Concetto R. Giuliano, Donald F. DuBois, and Gerald R. Rickel

HUGHES RESEARCH LABORATORIES  
*a division of hughes aircraft company*  
Malibu, California 90265

Contract No. F19628-69-C-0277  
Project No1 8693

Semiannual Report No. 4  
July 1971

*Approved for public release; distribution unlimited.*

Contract Monitor: Erlan S. Bliss, Capt., USAF  
Optical Physics Laboratory

*Sponsored by*  
Advanced Research Projects Agency  
ARPA Order No. 1434

Monitored by  
AIR FORCE CAMBRIDGE RESEARCH LABORATORIES  
AIR FORCE SYSTEMS COMMAND  
UNITED STATES AIR FORCE  
BEDFORD, MASSACHUSETTS 01730

**Details of Illustrations in  
this document may be better  
studied on microfiche**

## TABLE OF CONTENTS

ABSTRACT . . . . .	vii
LIST OF ILLUSTRATIONS . . . . .	v
I. EXPERIMENTAL STUDIES ON OPTICAL DAMAGE . . . . .	1
A. Introduction and Summary of Results . . . . .	1
B. Streak Camera Studies of Dynamics of Damage Filament Formation . . . . .	2
C. Damage Threshold as a Function of Beam Radius . . . . .	25
D. Damage with Cylindrical Lenses . . . . .	28
E. Beam Distortion in Ruby . . . . .	29
F. Ring Structure in the Focused Single Mode Laser Beam Beyond Beam Waist . . . . .	31
G. Plans for Next Reporting Period . . . . .	40
II. THEORETICAL STUDIES ON OPTICAL DAMAGE . . . . .	43
A. Introduction . . . . .	43
B. Kinetic Equation . . . . .	44
C. Approximate Considerations . . . . .	52
REFERENCES . . . . .	59
DD FORM 1473 . . . . .	61

## LIST OF ILLUSTRATIONS

Fig. 1.	Typical examples of damage tracks in sapphire caused by a temporally smooth pulse . . . . .	5
Fig. 2.	Examples of damage tracks in sapphire caused by temporally modulated pulse . . . . .	6
Fig. 3.	Schematic representation of laser and amplifier and associated monitoring apparatus . . . . .	8
Fig. 4.	Streak camera experimental setup . . . . .	11
Fig. 5.	Typical examples of damage filament, streak photograph, and oscilloscope trace for a temporally smooth incident pulse . . . . .	13
Fig. 6.	Typical example of damage filament, streak photograph, oscilloscope trace for a modulated ( $\sim 750$ MHz) incident pulse . . . . .	14
Fig. 7.	Juxtaposition of oscilloscope trace and streak photograph showing method of obtaining instantaneous powers and corresponding damage location . . . . .	16
Fig. 8.	Plot of $P^{1/2}$ versus $z_f^{-1}$ from data taken from streak and oscilloscope photographs . . . . .	19
Fig. 9.	Example of typical damage track in ruby caused by temporally smooth pulse . . . . .	23
Fig. 10.	Threshold power density versus beam radius for ruby and sapphire samples . . . . .	27
Fig. 11.	Schematic representation of setup used in beam profile measurements . . . . .	30

Fig. 12. Multiple lens camera photographs of beam profile inside ruby sample . . . . . 32

Fig. 13. Beam profile at different distances from 30.5 cm lens . . . . . 34

Fig. 14. On-Axis minimum in beam profile taken by placing scatterer directly in beam . . . . . 39

## ABSTRACT

In this report details of the temporal development of damage tracks are presented and discussed in terms of a self-focusing theory. The results of a number of streak camera photographs show that the damage track grows in a way which depends on the temporal behavior of the leading edge of the incident pulse. This work constitutes the first direct evidence for a moving self-focus in solids. A comparison with self-focusing theory is given and the importance of electrostriction is made evident. Damage thresholds in sapphire for lenses of different focal length are presented and compared with the results obtained for ruby in the last report. Also in this report damage with cylindrical lenses is discussed. It was not possible for us to generate damage using cylindrical lenses even though the power density was greater than ten times the power density required to reach damage threshold with a spherical lens giving the same focal spot area. This result suggests that self-focusing is sensitive to beam shape and may point to a possible solution to the problem of damage in high power laser devices. Also in this report an observation of rings in the beam profile of the focused laser beam is presented. The phenomenon which appears at points beyond the beam waist is a property of the ruby laser or possibly a combination of the laser and the lenses. This behavior could well be a general property of "single mode" solid state lasers. Further theoretical effort has been devoted to the problem of heating of electrons in polar crystals by intense optical fields. A kinetic equation has been developed which appears to offer a basis for settling the question of electron heating.

## SECTION I

### EXPERIMENTAL STUDIES ON OPTICAL DAMAGE

#### A. INTRODUCTION AND SUMMARY OF RESULTS

During this period we have performed a number of experiments in which we have studied the time evolution of damage tracks at different peak powers for two different pulse lengths. Results of these experiments have been compared with the self-focusing theory of Marburger and coworkers and a good picture of the dynamic details of damage formation has been obtained. This work forms the first direct evidence for a moving self-focus as being responsible for the initiation of filamentary damage. Results of damage threshold in sapphire and ruby using lenses of different focal lengths are presented. We also discuss the results of experiments in which we attempted to generate bulk damage using cylindrical lenses. We were unable to reach damage threshold under these conditions, even though the incident power was more than ten times higher than that required for a spherical lens that gives a focal spot of the same area as the cylindrical lens used. This suggests that self-focusing is sensitive to beam shape and may point to a possible solution to the problem of damage in high power laser devices.

Also during this period we performed experiments to further explore the beam distortion observed in ruby (discussed in Semiannual Report No. 3). The results of the experiments carried out with optically pumped ruby samples were inconclusive. Another phenomenon, characteristic of the ruby oscillator, was discovered during this period. We find that the beam profile exhibits rings and on-axis minima at points somewhat beyond the beam waist when the beam is focused.

This phenomenon may result from a combination of non-gaussian beam profile and a small amount of lens aberration. Nonuniform phase fronts of the laser beam is also suggested.

The theoretical effort during this period has concentrated on an attempt to understand, fundamentally, the heating of electrons in polar crystals by intense optical fields. The question still remains unanswered, but a kinetic equation has been developed which is believed to offer a fundamental basis for solving the problems of electron heating.

#### B. STREAK CAMERA STUDIES OF DYNAMICS OF DAMAGE FILAMENT FORMATION

The bulk of the experimental effort during this period has been devoted to a continuation of the streak camera studies with particular emphasis on sapphire. Many of the results obtained in the last report have been improved and a number of details, both qualitative and semi-quantitative, are understood in terms of self-focusing as the initiating mechanism for bulk filamentary damage. As mentioned in Semiannual Report No. 3, we have been in contact with J. H. Marburger of the University of Southern California, who has been working with the theory of self-focusing. A treatment of our experimental measurements in the framework of his theory has yielded a satisfying picture of the dynamics of self-focusing and its connection to the damage filaments. This collaboration has resulted in a manuscript submitted to Physical Review Letters and a presentation at the Third ASTM Symposium on Damage in Laser Materials, Boulder, Colorado, May 19, 20, 1971.

The manuscript of the paper to be published in the Proceedings of the ASTM Symposium is presented in the following section. The manuscript of the letter by Giuliano and Marburger contains most of the essential points of the following manuscript.

1. Time Evolution of Damage Tracks in Sapphire and Ruby\*

Concetto R. Giuliano

Hughes Research Laboratories  
Malibu, California 90265

ABSTRACT

A fast streaking camera has been employed to observe the time-evolution of bulk damage filaments in sapphire and ruby on a nanosecond time scale. Externally focused light from a mode controlled ruby laser and amplifier was used to induce damage in the samples studied. Either side-scattered light at  $6943 \text{ \AA}$  or blue-green light from the self-luminous damage sites was detected by the streaking camera. It was found that damage first occurs at or near the natural focus of the lens, and that the damage track grows in an upstream direction toward the laser. The damage filament is formed during the rising portion of the incident laser pulse, reaching its full length at the peak of the pulse. The relationship between the location of the damage at a given instant and the corresponding instantaneous laser power will be discussed in the context of a possible self-focusing mechanism.

Introduction

The causes of laser induced damage can be divided into three separate steps. First, the initiating step, in which the intensity is built up in the medium by a mechanism such as self-focusing. Second, the medium responds to these high intensities by undergoing any of a

---

\* This work was supported by the Advanced Research Projects Agency under ARPA Order 1434 with Air Force Cambridge Research Laboratories.

number of nonlinear processes such as multiphoton absorption and/or phonon generation. Third, the local power dissipation is high enough to exceed the elastic limits of the material, causing catastrophic breakdown.

Much indirect evidence has existed for supporting self-focusing as the initiating mechanism for laser-induced bulk damage.<sup>1,2</sup> However, different interpretations for the phenomenon have been postulated such as self-trapped filaments of light, repetitive focusing, and moving foci. We have observed the time-development of damage tracks in sapphire and ruby and found that it is most logically explained in terms of a moving focus. This is the first direct observation in support of a moving focus in solids.

We confine our discussion to the phenomenon of bulk damage in sapphire, although much of the discussion applies in general for most transparent dielectrics in which the filamentary damage is observed. The damage is characterized by a long track, as shown in Fig. 1. Here we see a typical damage track formed by a single pulse from a laser operating in a single longitudinal and transverse mode. The damage filament is characterized by a "head" at the part of the track nearest the sample entrance and a tapering "tail," the end of which occurs at or very near the focal plane of the lens used to focus the laser light in the material. The track often, but not always, displays a region of relatively dense damage at or near the tip of the tail, usually in the form of a crack or "damage star." As we examine the regions of the damage track upstream from the tail (Fig. 1(b)), we begin to see some subsidiary fracturing alongside the damage filament. This fracturing is randomly located and becomes increasingly dense toward the head of the track where the extent of subsidiary fracturing is maximum (Fig. 1(c)). If the incident light pulse is not temporally smooth, the damage track shows the same filamentary behavior, and in addition, there are occasional regions of more dense damage along the track. An example of this is shown in Fig. 2, where we see a track formed by a pulse

NOT REPRODUCIBLE

HRL546-5

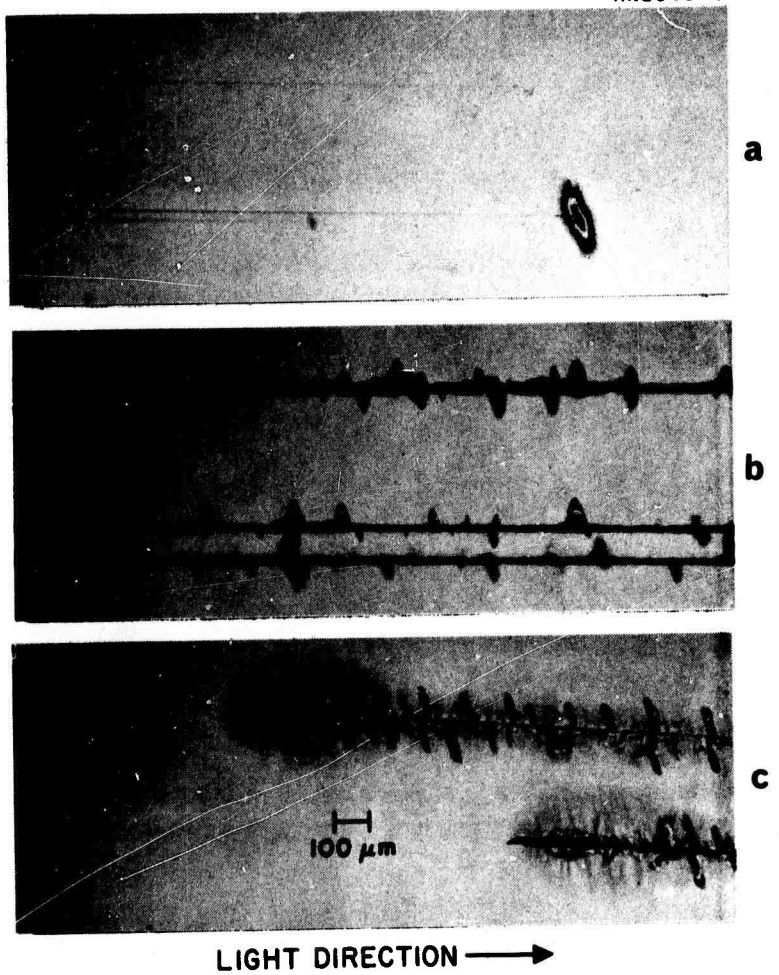
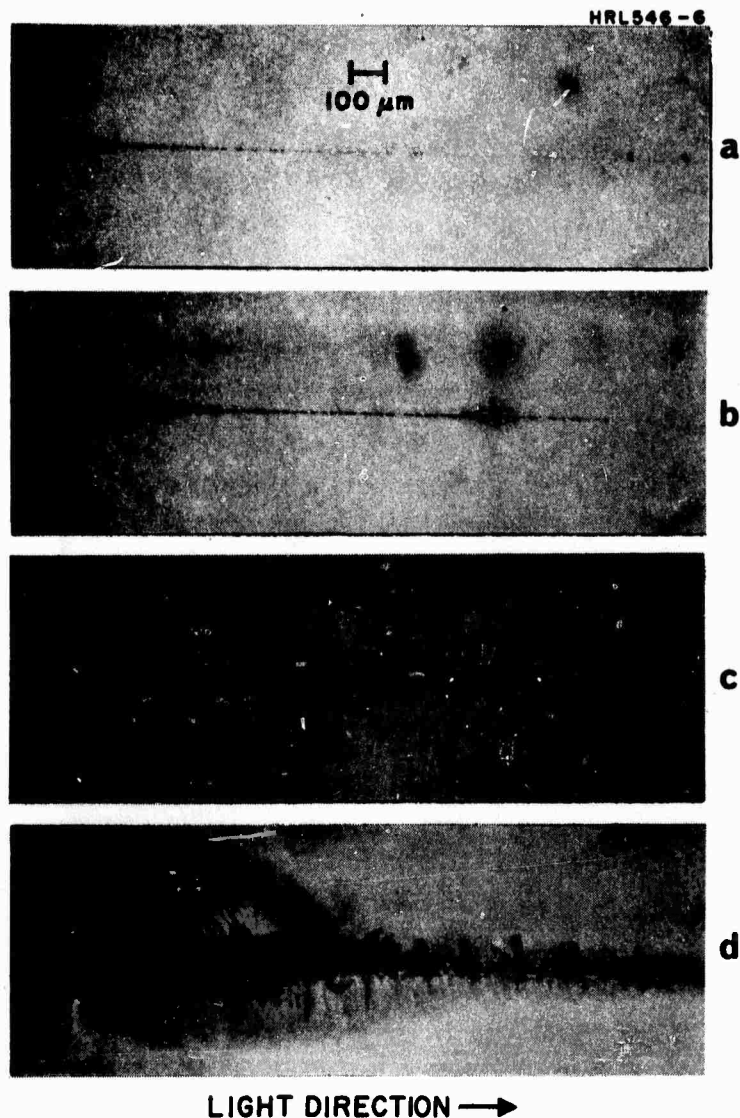


Fig. 1.  
Typical examples of damage tracks in sapphire caused by a temporally smooth pulse showing damage at (a) the tail, (b) the intermediate region, (c) the head.



NOT REPRODUCIBLE

Fig. 2.  
Examples of damage tracks in sapphire  
caused by a temporally modulated pulse,  
(a) through (d) progressing from the  
tail to the head.

in which the laser was oscillating in two longitudinal modes. If the depth of modulation of the incident pulse is large, the filamentary character of the damage track may not be present. Instead, one may see only a series of fractured regions spaced along the light path with gaps of undamaged material between them. We also notice the general feature that the damage filament itself is narrower at the tail of the track ( $\sim 2$  to  $5\ \mu\text{m}$ ) and broader at the head (several tens of microns). These qualitative features of bulk damage in the light of our recent observation of the time-evolution of these damage tracks will be explained.

### Experimental

The experimental setup is shown in Fig. 3. The oscillator employs a 4 in. long by  $1/4$  in. diameter ruby pumped by two linear lamps in a double elliptical pump cavity. The ruby crystal is water cooled by a closed-cycle refrigeration system maintained at  $0^\circ\text{C}$ . The high reflectivity mirror is coated with a 99+% reflectivity high field damage coating from Perkin Elmer Corporation. Q-switching is accomplished with a solution of cryptocyanine in methanol in a 1 mm path length cell whose transmission is 30% at  $6943\ \text{\AA}$ .

The temperature controlled ( $34^\circ\text{C}$ ) resonant reflector that was designed to optimize longitudinal mode control consists of two quartz etalons and a quartz spacer, whose combined effect is to enhance cavity modes separated by  $2\ \text{cm}^{-1}$  and to discriminate against intermediate modes.

Portions of the laser beam are split off in various ways (see Fig. 3), so the power output, near- and far-field patterns, and Fabry-Perot patterns can be monitored for each shot. This is accomplished in the following way. Light reflecting from wedged beamsplitter  $W_1$  gives two diverging beams. One beam hits the magnesium oxide

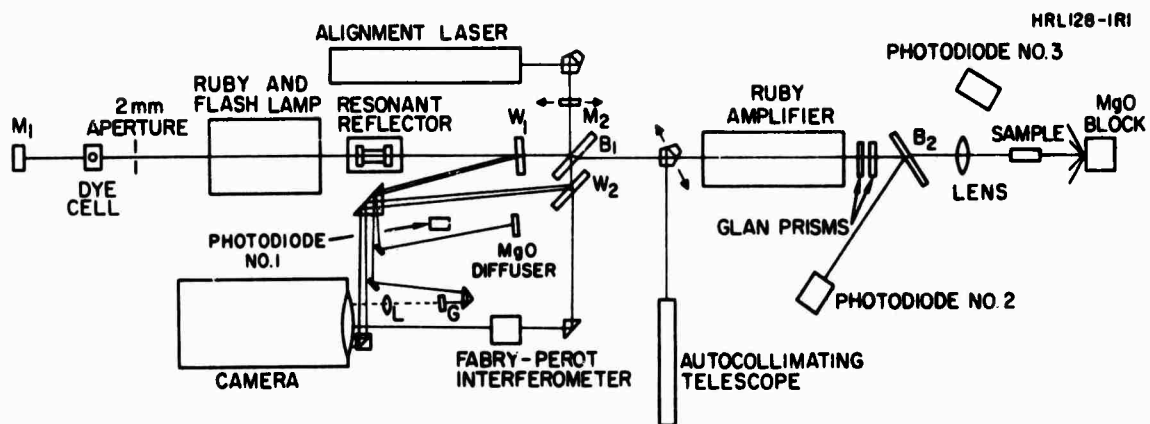


Fig. 3. Schematic representation of laser and amplifier and associated monitoring apparatus.

diffuser, where the scattered light is monitored by a biplanar photodiode used as our power monitor. The other beam from  $W_1$  hits ground-glass screen  $G$ , where it is photographed through lens  $L$  and the 1 m focal length camera focused at infinity. This gives a magnified ( $\sim 5x$ ) near-field picture. Another portion of the light is removed by beamsplitter  $B_1$  and hits mirror  $M_2$ , which can be placed in or out of position, depending on the use of the alignment laser. From  $M_2$  the light either goes to the Fabry-Perot interferometer or can be partially reflected from wedged beamsplitter  $W_2$ , where it results in a pair of far-field patterns. A 0.6 neutral density filter is placed near the focal plane of the camera so that the far-field pattern and the Fabry-Perot pattern can be seen at two different exposures. The two Glan prisms are used as a variable attenuator after the amplifier. Beamsplitter  $B_2$  samples the light to photodiode No. 2, which monitors the power incident upon the focusing lens, which was designed for minimum spherical aberration (Special Optics). Photodiode No. 3 monitors the light after the sample. The signals from the two detectors are integrated and displayed on a dual-beam oscilloscope.

The water cooled amplifier ruby is 6 in. long x 0.5 in. diameter, with one end wedged relative to the other by about  $0.5^\circ$ . The input end of the amplifier rod is antireflection coated to minimize the chances of oscillation within the amplifier itself. The ruby rod is closely coupled to a helical flashlamp, which is pumped with a power supply capable of delivering 8 kJ in a 3 msec pulse. The power supply employs a pulse shaping network of 20 sections, each section pumping for 150  $\mu$ sec. The maximum gain obtained with the amplifier is about 10 dB.

In all experiments described in this section, the amplifier flashlamp pumping was held constant, and the amount of light incident on the sample was varied by rotating the first of the two Glan prisms. We have found that our amplifier acts as a weak negative lens whose focal length depends on optical pumping.<sup>3</sup> Thus, we fixed the amplifier pumping to

minimize the shot-to-shot variations in the beam characteristics.

Typical output from the oscillator plus amplifier is  $\sim 150$  mJ in pulses which can range from about 15 to 30 nsec. The far-field beam profile was measured to be gaussian down to 8% of the peak using a modified multiple-lens camera technique.<sup>4</sup>

The streak camera experimental setup is shown in Fig. 4. We used an STL image converter camera operating in the streaking mode to photograph the self-luminous damage tracks during their formation. The camera was triggered either by the sync pulse from the Pockels cell, when it was used as the Q-switch, or from the laser light itself, when the cryptocyanine Q-switch was employed. For all the experiments described, the light was focused inside the sample using a lens ( $f = 19$  cm) which was designed for minimum spherical aberration. In the latter experiments a portion of the incident light was split off and allowed to enter the camera directly to give a marker streak which gives the relation between the time of formation of a particular point on the damage track and the peak of the incident pulse. In the experiments described here, a Corning 4-94 filter was placed in front of the camera lens. This served to block the laser light which was scattered from the damage sites while passing the self-luminous light in the blue-green part of the spectrum. When the scattered light at  $6943 \text{ \AA}$  is allowed to enter the camera, essentially the same behavior is observed when it is blocked. However, scattered laser light from previously formed damage tracks in the sample constitutes an inconvenient background which interferes with the observation of the track of interest. After each streak photograph was taken, the position of the head and tail of the damage track was determined by examining the crystal using a measuring microscope. These measurements were found to be consistent with the location and extent of the damage inferred from the streak photos.

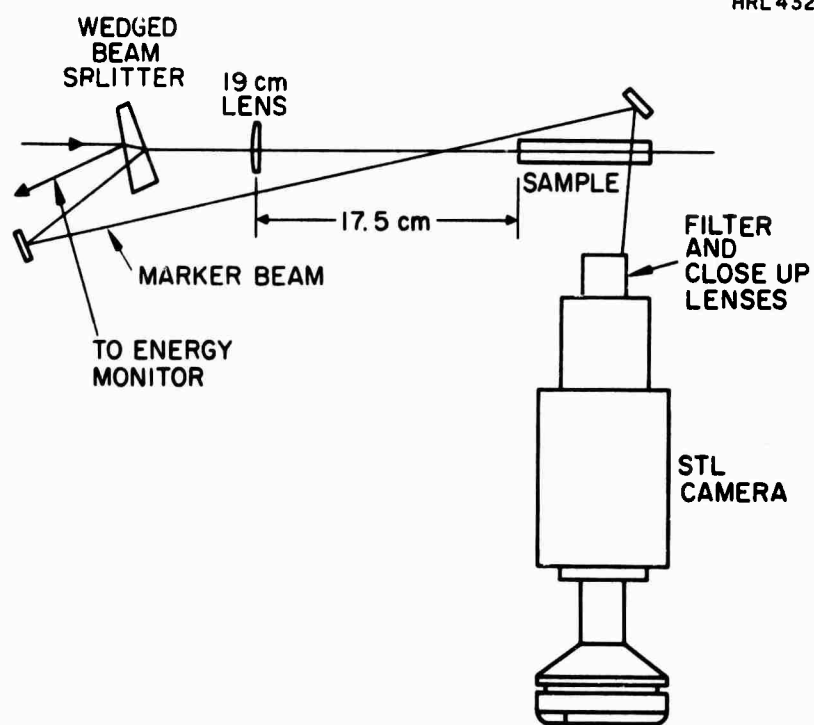


Fig. 4. Streak camera experimental setup.

## Results of Streak Measurements

Typical streak photographs of the damage in sapphire are shown in Figs. 5 and 6. Figure 5 shows the time development of the damage track when an unmodulated pulse is incident on the sample. In Fig. 6 we see the streak photo for a modulated input pulse. (The 750 MHz modulation occurs when the Pockels cell Q-switch is used.) Essential features of these results are

- The track first appears at or very near the location of the beam waist\*
- The track grows in the upstream direction moving toward the sample entrance
- The track reaches its maximum length when the incident pulse reaches its peak.

The qualitative behavior of the time evolution of these damage tracks can be described in terms of moving self-focus as follows. At a certain critical power  $P_c$ , a self-focus first appears at the beam waist where the damage first occurs. As the power increases the distance  $z_f$  required to form a self-focus decreases, and the damage track grows in the upstream direction. The minimum  $z_f$  corresponds to the maximum power; thus the head of the track will occur at the peak of the incident pulse. The rate of growth of the track depends on the temporal shape of the laser pulse. The self-focused spot sweeps through the downstream part of the track more rapidly than the upstream part, making the extent of damage greater at the head than at the tail.

When the incident pulse is modulated, we expect to see local regions of heavy damage associated with the passage of local maxima on

---

\*In many of the photographs the intensity of the light from the tail of the track is too weak to record. However, subsequent examination of the tracks show that the location of the tail is highly reproducible from shot to shot.

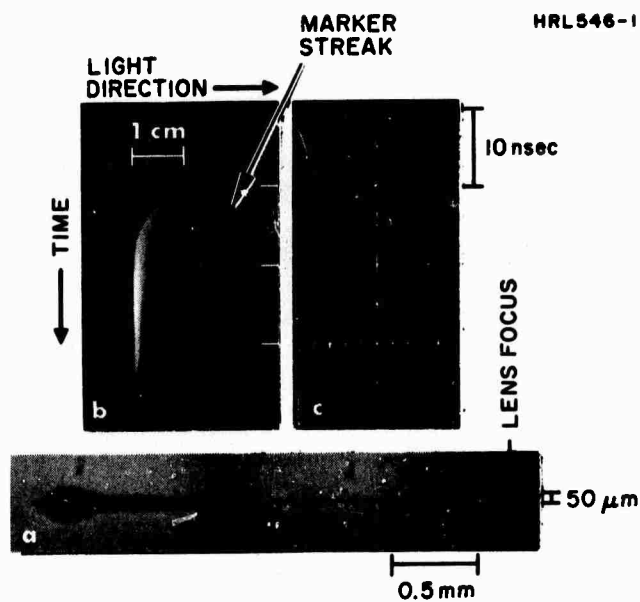


Fig. 5.  
 Typical examples of (a) damage  
 filament, (b) streak photograph,  
 (c) oscilloscope trace for a  
 temporally smooth incident pulse.

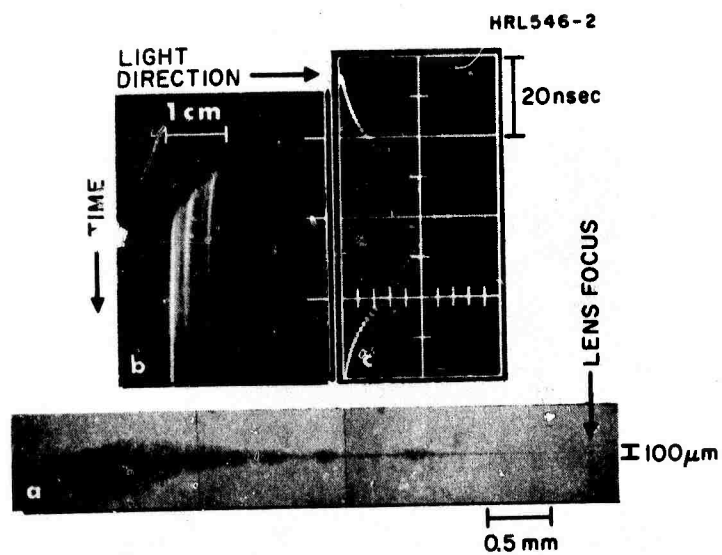


Fig. 6.  
 Typical example of (a) damage  
 filament, (b) streak photograph,  
 (c) oscilloscope trace for a  
 modulated ( $\sim 750$  MHz) incident  
 pulse.

the leading edge of the pulse. Each consecutive peak has slightly more power than the preceding one, and therefore causes a self-focus which dwells at slightly smaller  $z$ . A glance at the damage track formed from a modulated pulse (Fig. 6) shows the spacing between the heavily damaged regions to decrease toward the head of the track, as one might expect from the above qualitative explanation. Thus, what might appear to be evidence for multiple or repeated focusing could be simply an artifact of temporal spiking on the input pulse, which causes a single focus to pause occasionally as it sweeps upstream.

Streak photographs of damage tracks in ruby show the same qualitative behavior as that seen in sapphire, but the comparison with the self-focusing theory below was not carried out. The general features of damage in ruby are not the same as those in sapphire, and the location and lengths of damage tracks are not as reproducible. This may be attributed to the absorption in ruby at  $6943 \text{ \AA}$ , but the differences have not been investigated in detail (see Ref. 3).

The reduction of data taken from streak and oscilloscope photographs was accomplished by tracing the photographs onto graph paper at a convenient magnification, using an opaque projector and picking off values of instantaneous power and damage location at specific times. The two time scales were synchronized by locating the center (most intense region) of the marker streak and allowing this to coincide with the peak of the incident laser pulse. The center of the marker streak was determined "by eye" and was found to be reproducibly locatable to within about 1 nsec (1 mm on the streak photographs). Thus, we obtain values of distance of a particular point on the damage track from the entrance surface  $z_f$  and the corresponding instantaneous laser power. An example of the traces is shown in Fig. 7.

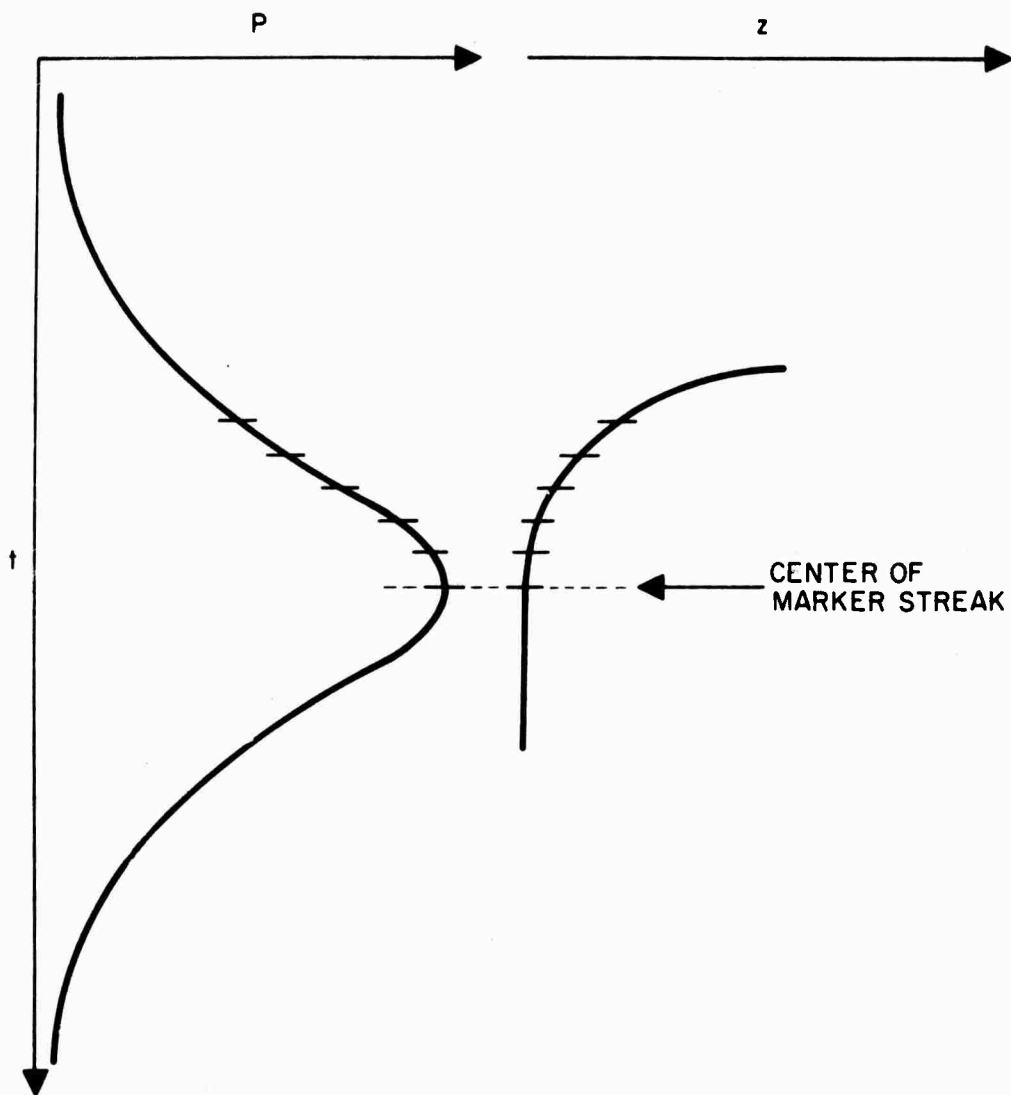


Fig. 7. Juxtaposition of oscilloscope trace and streak photograph showing method of obtaining instantaneous powers and corresponding damage location.

## Comparison of Experiment with Theory

We will now attempt to correlate the above experimental results with the self-focusing theory of Marburger and coworkers.<sup>5, 6</sup> Many of the details of this theory are presented in a following paper.<sup>7</sup>

The above referenced theory assumes that the induced refractive index in the medium  $\delta n$  responds instantly to local changes in the optical intensity. The following equation is obtained from numerical solutions of the nonlinear wave equation (for  $P > P_c$ ).

$$\left( (P/P_c)^{1/2} - 0.858 \right)^2 = 0.0202 + 0.136 \left[ k a_0^2 / z_f(\infty) \right]^2 \quad (1)$$

and

$$z_f^{-1}(\infty) = z_f^{-1}(R) + R^{-1} \quad (2)$$

Here, for an incident gaussian equiphase beam,  $a_0$  is the  $e^{-1}$  radius of the intensity profile at the sample entrance,  $k$  is the wave vector in this medium,  $R$  is the distance from the crystal entrance to the low intensity beam waist,  $z_f(R)$  is the distance from the sample entrance to the self-focus when the incident beam has phase curvature  $R$  ( $R < 0$  for a converging beam);  $P$  and  $P_c$  are the incident power and the critical power for self-focusing, respectively. The theory predicts that two self-foci are formed; they coincide at the low intensity beam focus at  $P = P_c$  and at higher power they separate, one moving downstream at the speed of light and the other moving upstream at a rate which depends on the temporal shape of the input pulse. We will deal here with a comparison of the theory and experiment for the backward moving self-focus.

Equation (1) is a hyperbola whose asymptote is

$$(P/P_c)^{1/2} = 0.858 + 0.369 k a_o^2 \left( \frac{1}{R} + \frac{1}{z_f(R)} \right). \quad (3)$$

Thus, for powers greater than  $\sim 2P_c$ , a plot of  $P^{1/2}$  versus  $z_f^{-1}$  should give a straight line. Figure 8 shows that this is nearly so. Here we present data taken from a number of streak camera measurements for different peak powers and at two different pulse widths  $\tau$ .

The evident curvature of the plots in Fig. 8, and their dependence on peak power and pulse duration, can be explained by including the slow response of the index change  $\delta n$  which was ignored in the above analysis.

Of the various possible mechanisms for  $\delta n$ , those arising from nonlinearity of electronic response<sup>8</sup> and libration<sup>9</sup> are essentially instantaneous. The largest noninstantaneous mechanism for  $\delta n$  is electrostriction, which leads to an effective nonlinear index of refraction  $n_2$ , decreasing as the dimensionless quantity  $x = a/u\tau$  increases.<sup>10</sup> Here,  $a$  is the spatial beam radius,  $\tau$  is the effective pulse width, and  $u$  is the longitudinal sound velocity in the medium. Thus, there is a characteristic time  $a/u$  for the electrostrictive nonlinearity to develop, and hence the critical power required to obtain a self-focus will depend on beam size and pulse duration.

The index change leading to a self-focus at a particular distance  $z_f$  can only be induced by that portion of the pulse which has passed  $z_f$  before the self-focus is formed. Thus the effective  $\tau$  should be considered a decreasing function of  $z_f$  when considering points along an evolving damage track formed on the leading edge of the pulse. For a converging beam, the beam width  $a$  increases with decreasing  $z$ . Thus, it becomes increasingly difficult for electrostrictive self-focusing to occur as  $z_f$  decreases for a given input pulse; a self-focus formed upstream from the low intensity beam waist cannot take advantage of the small beam radius at the natural focus.

We can roughly account for the effect of electrostriction by replacing  $P_c^{-1}$  in eq. (1) by  $P_{c1}^{-1} + [P_{c2}f(x)]^{-1}$ , where  $f$  is an

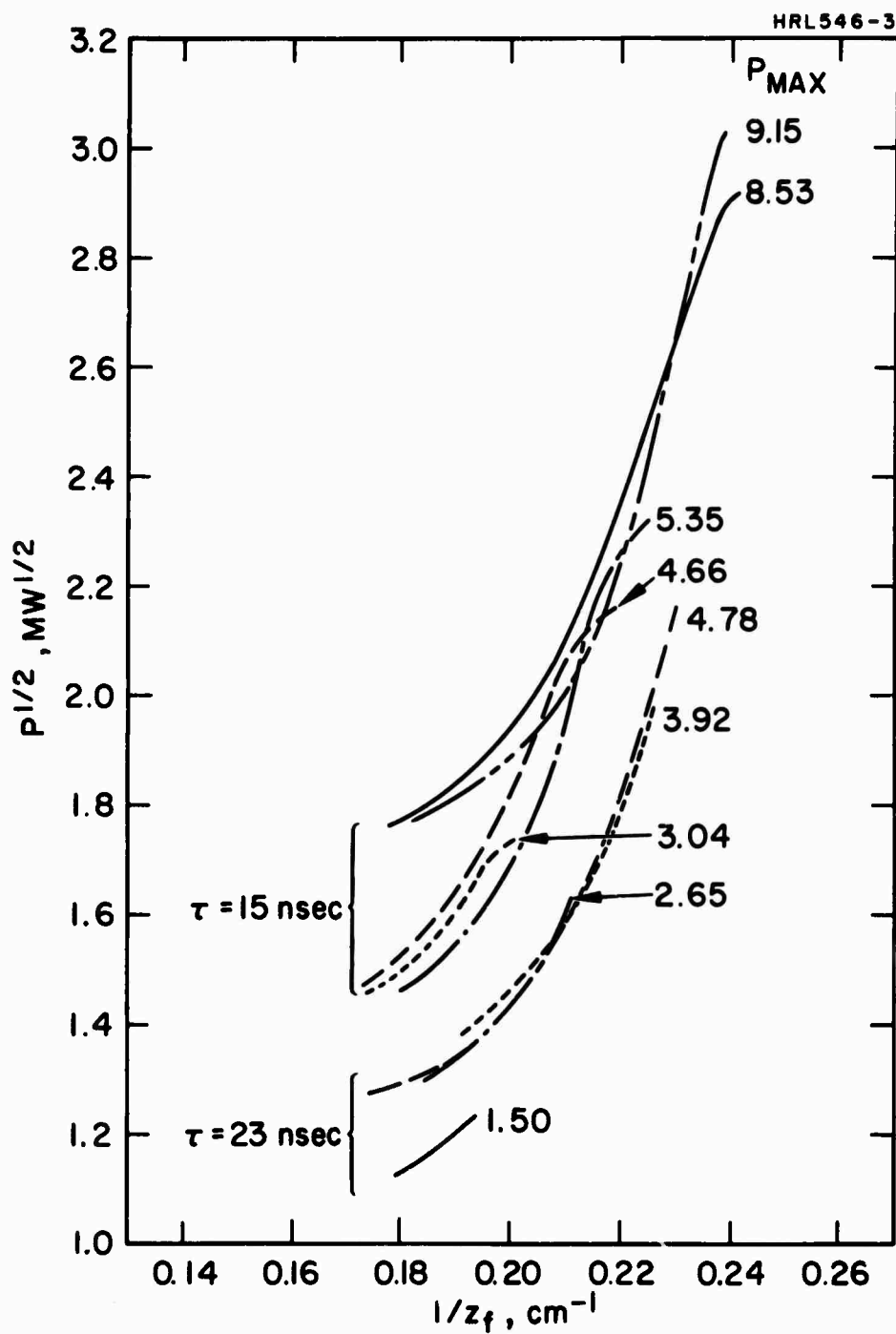


Fig. 8. Plot of  $P^{1/2}$  versus  $z_f^{-1}$  from data taken from streak and oscilloscope photographs for different incident peak powers and pulse widths.

increasing function of  $x$ ,  $P_{c1}$  is the critical power due to instantaneous mechanisms, and  $P_{c2}f(x)$  is the critical power for electrostriction.

For our particular conditions of pulse lengths and focusing, the fractional change in  $a$  from the tail to the head of the track is substantially larger than the fractional change in  $\tau$ . Therefore, we expect  $f(x)$  to be a decreasing function of  $z_f$ , causing positive curvature in a plot of  $P^{1/2}$  versus  $z_f^{-1}$  according to eq. (1). This is consistent with the data shown in Fig. 8.

Since the first self-focus occurs at the low intensity beam focus,  $a$  is the same for all curves at  $z_f = |R|$ . Therefore, we would expect  $x$  to decrease for pulses of longer duration. As a result, the self-focus forms more easily (i. e., at lower powers) for a longer pulse, everything else being equal. This explains the vertical separation between the two groups of curves in Fig. 8. Similarly, one would expect that pulses of different peak power, but the same duration, would form an initial self-focus at different incident powers. In this case the critical power is less for lower peak power than for higher peak power pulses of the same duration. For example, when an incident pulse for which the self-focus occurs just at the peak is compared with a pulse of the same width but much higher peak power, one would expect the self-focus to first occur at a higher power for the latter pulse, because not enough time would have elapsed for a self-focus to have occurred at the same power as for the first pulse. This accounts for the separation at the low power end between curves of the same pulse width in Fig. 8.

The slight negative curvature seen at the high power ends of the curves in Fig. 8 is very sensitive to the "synchronization" of the pulse profile with the streak photographs. Because of the slow response of the electrostrictive mechanism, the maximum upstream excursion of the damage track would be expected to lag the pulse peak by an amount somewhat less than the response time. We did not attempt to consider this in plotting the data. This could explain the negative curvature seen at the high power ends of several of the curves in Fig. 8. A relative

shift between the oscilloscope traces and the streak photographs of the order of nanoseconds will remove this curvature. The direction of the adjustment is consistent with this explanation.

We see from eq. (3) that the straight line plot of  $P^{1/2}$  versus  $z_f^{-1}$  should have a slope of  $0.369 ka_0^2 P_c^{1/2}$ . Hence, we can obtain values for  $P_c$  from the slopes of the curves in Fig. 8. The value for  $a_0$  at the crystal entrance ( $1.85 \times 10^{-3}$  cm) was obtained by measurement of the beam profile at a number of points beyond the focusing lens. The range of critical powers obtained from the slopes in Fig. 8 is 180 kW to 5.4 MW, corresponding to values of  $n_2$  of  $9.5 \times 10^{-13}$  esu and  $0.31 \times 10^{-13}$  esu.\* These values are consistent at one extreme with the predictions of electrostrictive self-focusing theory for sapphire<sup>10</sup> (368 kW) and at the other with values of  $n_2$  arising from electronic nonlinearities in glass ( $n_2 = 1.8 \times 10^{-13}$  esu) (Ref. 11).

## 2. Dynamics of Track Formation in Ruby

The results obtained with ruby are qualitatively similar in some respects to those of sapphire. However, there are usually a few differences which emphasize a definite contrast between the damage phenomena in both materials. The quantitative comparison of the dynamical data is not available at this time, because the streak photographs for ruby damage are not defined as well as those for sapphire. Because the length of the damage track in ruby is about 1/3 as long as that in sapphire for the same incident power and focusing, the resolution in the streak photographs is less for the same magnification. In addition, the full length of the track in ruby generally is not visible in the streak photographs, since the downstream end does not glow brightly enough to be detected. Consequently, the visible portion of the tracks is very short and at the magnification used it is very difficult to make reliable measurements from the streak photographs.

---

\*These are obtained from the relation  $P_c = (1.7 \times 10^{-13}/n_2)$  MW.

In addition to the difference in track length, another feature that distinguishes ruby from sapphire is that the track in ruby is not a continuous filament even when the incident pulse is temporally smooth. An example of this is given in Fig. 9. This phenomenon is one of many distinctions between ruby and sapphire damage, which might be linked to the absorption in ruby, yet remain unexplained.

### 3. Further Discussion of Theory Compared with Experiment

The conclusion that the damage under the conditions of our experiments is the result of a moving self-focus rather than a trapped filament or a repetitive focus is an essential feature of this work. A close quantitative agreement with the self-focusing theory of Marburger and coworkers would predict that all the curves in Fig. 8 would lie on top of one another and be essentially coincident with the curve of eq. (1), substituting the proper values of  $a_0$ ,  $R$ , and  $P_c$ . Obviously, this is not the case, but the reasons are qualitatively understood, and a plausible explanation for the differences between the curves lies in the consideration that the nonlinearity does not respond instantaneously to the optical fields. The curvature of the plots, the shift between the two sets of curves for different pulse widths, and the differences in the low power ends of the curves with the same pulse width can be qualitatively understood by invoking a noninstantaneous response. In attempting to account for this empirically,  $P_c^{-1}$  in eq. (1) may be replaced by  $P_{c1}^{-1} + [P_{c2}f(x)]^{-1}$ , where  $P_{c1}$  is the critical power for an instantaneous response, and  $P_{c2}f(x)$  is the critical power for electrostriction. As mentioned in the manuscript  $f(x)$  is essentially a function which makes it harder to get self-focusing if the pulse is short or if the beam size is large. This says then, that for focused beams self-focusing becomes more difficult as the track progresses back toward the entrance, at least for pulses of roughly the width and temporal shape that we are concerned with.

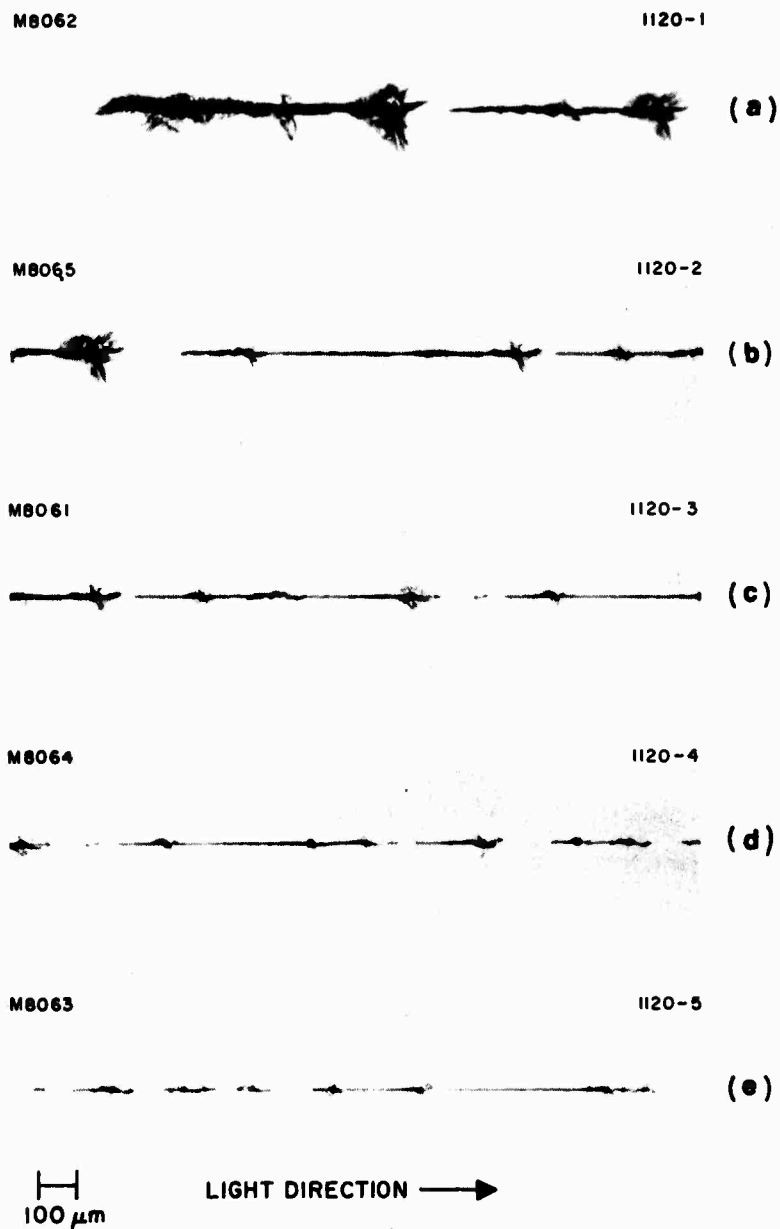


Fig. 9. Example of typical damage track in ruby caused by temporally smooth pulse ( $f = 19$  cm lens), (a) through (e) progressing from tail to head. Note breaks in damage track in contrast to unbroken track in sapphire.

It should also be pointed out that the theoretical treatment applies for gaussian beams with uniform phase fronts. This is not precisely true for our laser, or possibly for any solid state "single mode" laser. The deviation from gaussian character was pointed out in Semi-annual Report No. 3. Phase variations across the beam are suggested by the rings seen in the beam profile photographs discussed in Section F of this report

The extent to which the coefficients or the functional form in eq. (1) may be sensitive to these parameters is not known at this time. However, it may be possible with our present data to determine  $f(x)$ , thus obtaining a more satisfactory quantitative agreement than exists at this time.

#### 4. Summary of Streak Camera Experiments

In summarizing essential results of the dynamics of formation of the damage filaments, there are several important features on which the theory and experiment agree.

As the incident power reaches a critical value, a self-focus occurs at the low power lens focus. This is the first point where a self-focus is expected to occur. As the power is increased the distance necessary to obtain a self-focus is less, and the self-focus moves toward the entrance of the medium. Therefore, the damage track has one end at, or very near the lens focus and the other end between the focus and the crystal entrance. The rate at which the self-focus moves, and consequently, the rate at which the damage filament grows depends on the rate of change of intensity with time. The faster the intensity grows, the faster the self-focused spot moves upstream. When the incident pulse reaches its peak, the damage track reaches its maximum length. As the intensity decreases, the self-focused spot will tend to move back downstream. However, since the damage has already been

created, it interferes with the propagation back downstream. As a result, the head of the track shows more heavy damage. If the amplitude of the incident light pulse varies with time, the self-focused spot will move in an irregular fashion, going rapidly upstream when the intensity is rapidly increasing and pausing at local peaks. The damage resulting from this kind of pulse will show local regions of more heavy damage, formed during local maxima, separated by narrow filaments, formed when the self-focus was moving rapidly. If the depth of modulation is large, the connecting filamentary characteristic may not be observed, but only the regions of high local damage along a line separated by regions of no damage. Thus, what appear to be evidence for repetitive or multiple focusing can be shown to be a result of temporal structure on the rising portion of the input pulse.

#### C. DAMAGE THRESHOLD AS A FUNCTION OF BEAM RADIUS

In Semiannual Report No. 3 we presented the results of some measurements of bulk damage threshold in ruby for different focal length lenses. During this period we have performed similar experiments on sapphire and obtained similar results. The data are plotted in Fig. 10 as a log-log plot of threshold power density versus beam radius, both evaluated at the beam waist inside the sample. A slope of minus two in these plots would indicate a constant power threshold, independent of lens focal length that is consistent with a self-focusing mechanism in a material with an instantaneous nonlinear response such as that arising from electronic distortion. Instantaneous response implies that the steady state conditions for self-focusing apply. In the case of electrostrictive self-focusing as a dominant mechanism, this would correspond to long pulses or small beams. For pulses of constant length, the steady state condition for electrostriction is approached as the beam size gets smaller. The case of large beams or short pulses corresponds to the transient situation for electrostrictive self-focusing.

In the extreme of the transient regime, a constant power density threshold is expected, giving a slope of zero for large beam sizes in the plot in Fig. 10. If self-focusing by electrostriction were the sole cause of bulk damage, we would expect to see a slope of minus two in the small beam radius region, tailing off to zero slope at large radii. A combination of contributions from both slow and fast self-focusing mechanisms would give a slope less than minus two which we observe.

Of course, the above discussion really applies to situations where the light incident on the medium is unfocused, or slightly focused, because the self-focusing phenomenon depends on a nonlinearity which takes place continuously along the beam. That is, the phenomena which take place at a certain plane affect the self-focusing at points farther downstream in the material.

What will be expected then for sharply focused beams compared with gently focused beams? If the beam is sharply focused inside a material which is long compared with the length of the focal region, the beam size is rapidly decreasing with distance on the approach to the low power focus. This means that the region over which a phenomenon such as electrostriction is effective in creating self-focusing is less than if the beam radius were constant and the same size as at the waist. The material responds to create a kind of continuous acoustic lens all along the beam. But for a certain range of radii the ease with which the lens forms depends on the beam radius. Therefore, for a converging beam, electrostriction might be expected to be less effective as the external focusing becomes sharper. In a sense, then, one again enters a region corresponding to transient behavior. Here damage threshold would be expected to occur at a constant power density independent of lens focal length. For very sharply converging beams, damage is expected to occur before electrostrictive self-focusing has a chance to develop. The tailing off of the curves at small radii (i. e., sharp focusing) in Fig. 10 could be explained in terms of the behavior described

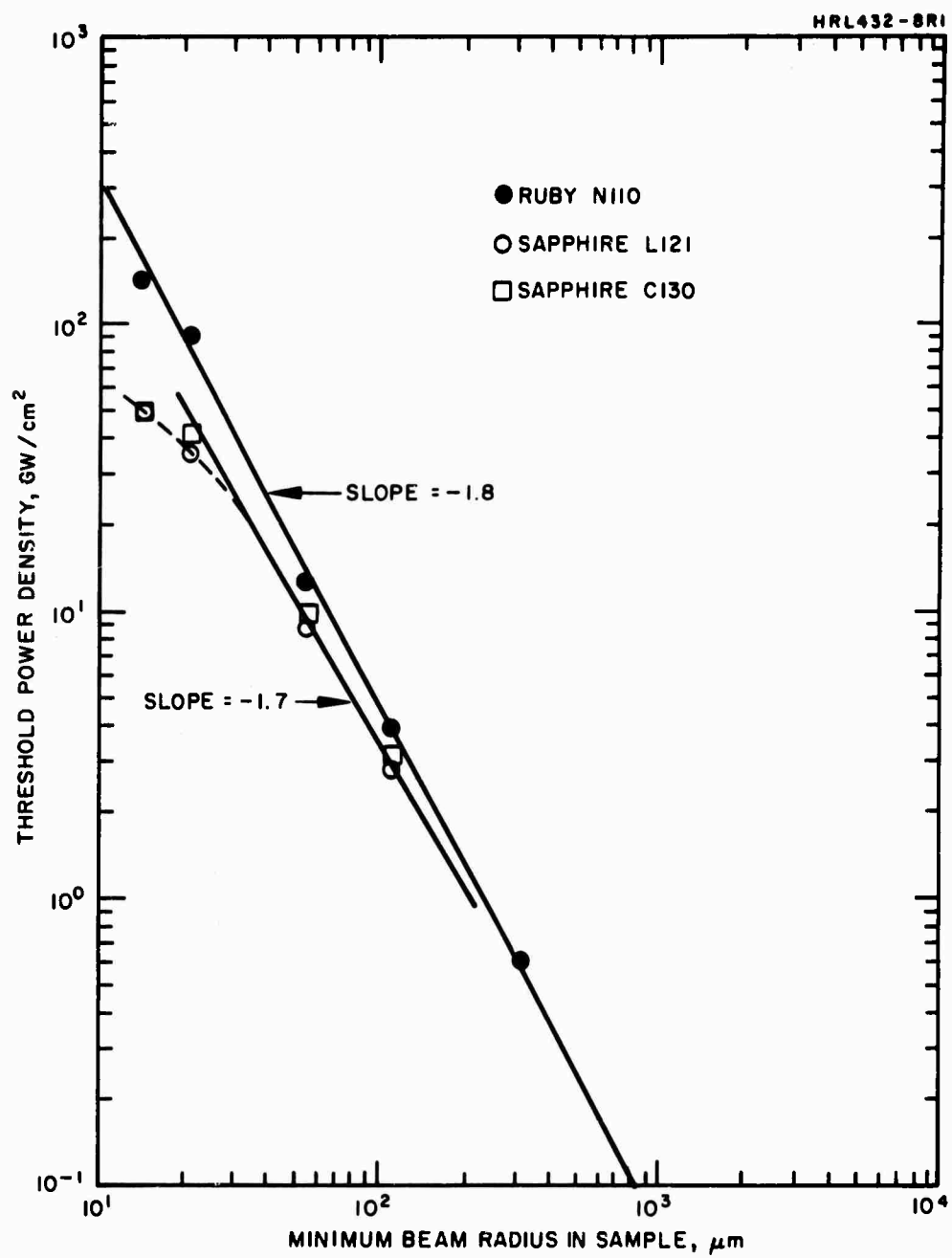


Fig. 10. Threshold power density versus beam radius for ruby and sapphire samples.

above. No suggestion of a change in slope for large radii is observed, apparently because the experimental conditions do not extend into the region of large enough beam size.

#### D. DAMAGE WITH CYLINDRICAL LENSES

During the latter part of this reporting period we have performed experiments with cylindrical lenses. The original intent of these experiments was to see whether the bulk damage would appear to be a sheet rather than a single filament, or whether the damage might appear to be a series of parallel filaments of perhaps different lengths. These ideas were based on a preconceived notion that at first sight would lead one to conclude that although a self-focus for a spherical lens is a point, the self-focus for a cylindrical lens would be a line, or perhaps a series of points if one allows for some breaking up of the beam.

This curiosity concerning the result of self-focusing of a beam focused by a cylindrical lens had a surprising result. We were unable to observe any damage in sapphire samples using a number of cylindrical lenses of relatively short focal length (as low as 7 cm for a pair (10 cm and 20 cm) of relatively good quality cylindrical lenses, and 3 cm for a lens of uncertain quality). We calculate power densities at the focus in excess of  $26 \text{ GW/cm}^2$  for which no damage is observed. This is computed on the basis of an elliptical spot with major and minor radii of 0.17 and  $1.17 \times 10^{-3}$  cm, respectively, and a pulse with a peak power of 16 MW and a duration of 14 nsec. We know from our previous experiments with spherical lenses that the damage threshold power density is a function of spot size in the sample. For focal spots of comparable area the damage threshold using a cylindrical lens is more than ten times higher than with a spherical lens. Since we have not seen any damage with the maximum output from our system, we cannot determine the actual ratio of thresholds at this time.

We have not yet considered the details of what one might expect for self-focusing of a beam that is not circularly symmetric or that tends to spread more rapidly in one direction than in another. The experimental results, however, strongly suggest that self-focusing depends on beam shape.

This result suggests an interesting possibility for avoiding damage in a number of applications. For example, phenomena which depend on power density such as second harmonic generation, should be unaffected by the shape of the beam. If higher power operation of laser devices could be obtained simply by changing the beam shape, it would be a welcome solution that would be relatively easy to carry out.

We will perform further experiments in this area during the next reporting period and also examine the theory of self-focusing for non-circularly symmetric beams.

#### E. BEAM DISTORTION IN RUBY

The problem of beam distortion in ruby is still unsolved. We carried out experiments in which we looked at the beam profile inside a ruby sample while optically pumping the sample. The results were inconclusive.

Let us summarize the result of this beam distortion as discussed in the previous report. Figure 11 describes the focusing lens and imaging lens setup we used to image a plane inside the sample onto the MgO block. The lenses and samples were placed so the waist of the focused beam would occur about 2 cm inside the exit surface of the 3 in. long sample. The plane being imaged was about 0.5 cm upstream from the beam waist. The ruby laser and amplifier were operated to give essentially a constant power output and the power incident on the sample was varied by rotating the first of a pair of polarizing prisms located after the amplifier.

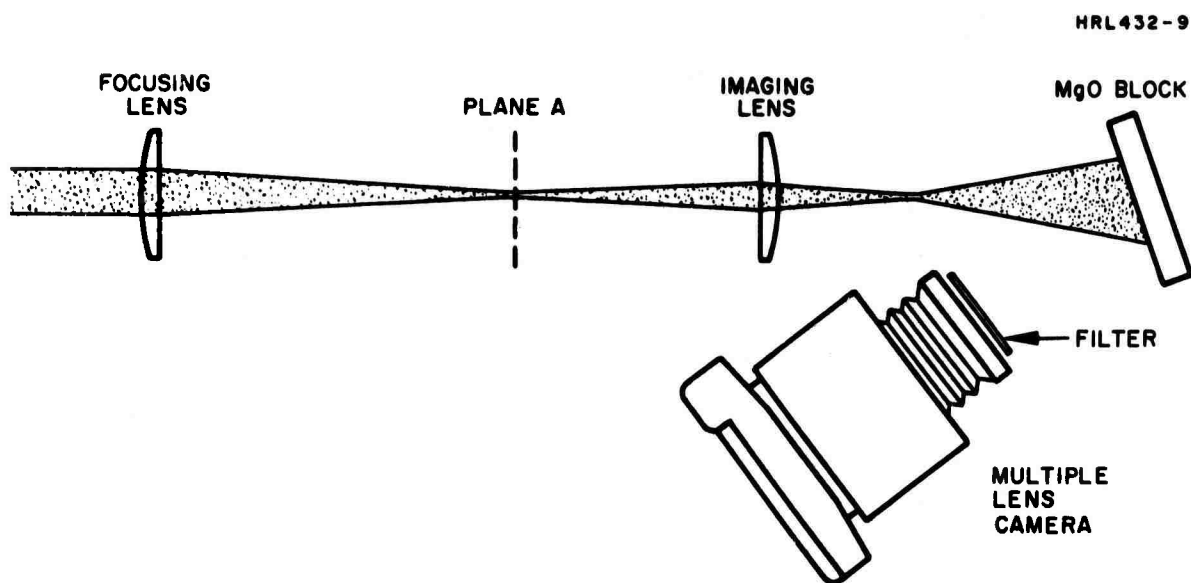


Fig. 11. Schematic Representation of Setup Used in Beam Profile Measurements.

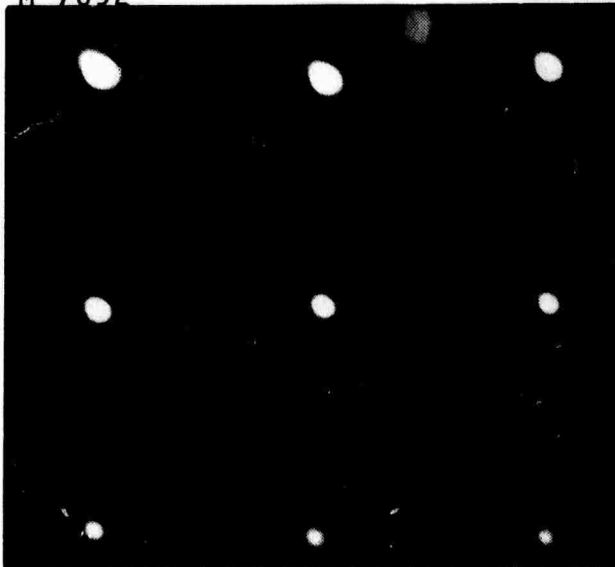
We found that at low incident energy ( $\sim 0.3$  mJ) the beam profile appears smooth but that as the incident energy is increased (greater than  $\sim 3$  mJ), the beam profile shows some irregular characteristics such as bright central spots, rings, and minima. These results are illustrated in Fig. 12. We wish to re-emphasize that this behavior that occurs well below damage threshold in ruby is not observed in sapphire at powers up to and beyond the bulk damage threshold.

Because the obvious difference between sapphire and ruby at  $6943 \text{ \AA}$  is the optical absorption, we decided to look at the beam profile inside pumped ruby samples to see whether the same distortion is seen under these circumstances. We chose an incident power level where the distortion is pronounced in an unpumped sample and optically pumped the sample at different levels. The results were inconclusive, because while the beam profile definitely changed with optical pumping, there was no marked improved or lessening of the distortion that could be directly attributed to the pumping. At the time these experiments were carried out we were having difficulty with oscillator and amplifier alignment fluctuations, which also gave rise to distinct beam profile irregularities. It was not possible at the time to separate effects arising from a possible misalignment variation from shot to shot. This lack of reproducibility of results from shot to shot and from day to day made it impossible to reach any definitive conclusion concerning the effects of optical pumping on the beam distortion in ruby. At this time the question still remains unanswered.

#### F. RING STRUCTURE IN THE FOCUSED SINGLE MODE LASER BEAM BEYOND BEAM WAIST

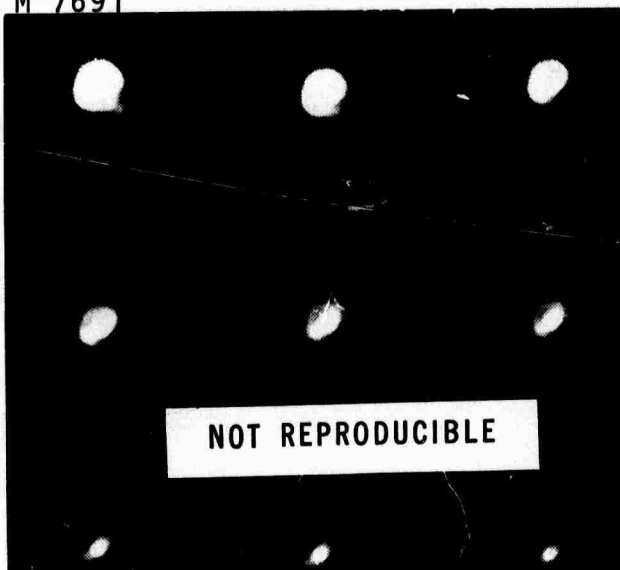
Our plans to examine in more detail the beam distortion effect in optically pumped ruby samples were preceded by preliminary experiments in which the ruby sample was absent from the beam. During these

M 7692



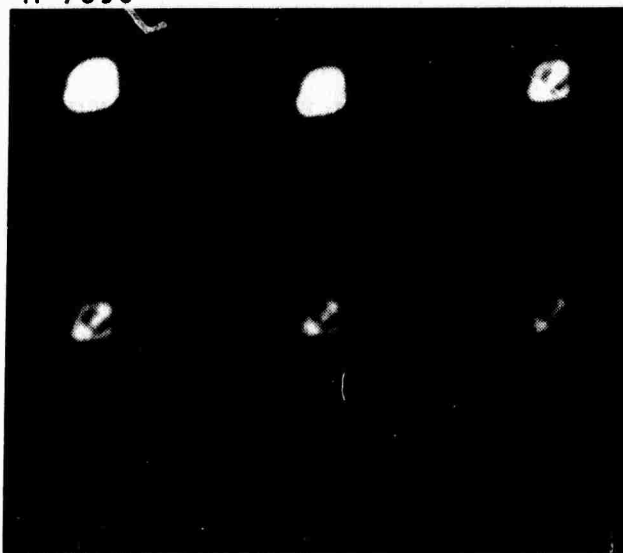
(a) 0.33 mJ

M 7691



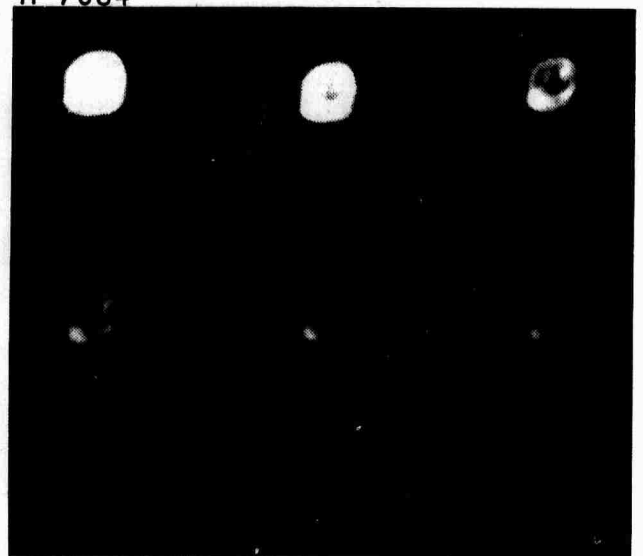
(b) 3.0 mJ

M 7690



(c) 5.1 mJ

M 7684



(d) 10.5 mJ

M 7685



(e) 10.8 mJ

Fig. 12.  
Multiple Lens Camera Photographs of Beam Profile Inside Ruby Sample for Different Incident Energies and Arbitrary Relative Exposures. (Constant amplifier pumping - 150  $\mu$ F, 7.5 kV.)

experiments we obtained an unexpected result which diverted us from our original objective and which we pursued further to understand its origin. We will describe the results of these observations in this section.

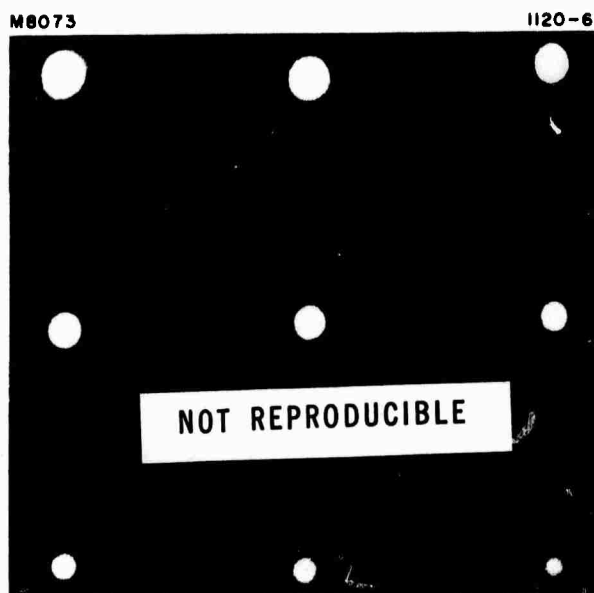
We wish to point out that the phenomena to be described were observed with only the light from the laser. No other elements are placed in the beam between the oscillator output mirror and the lenses except for beam splitters and polarizer attenuators; the removal of these does not change what was observed. Also, the presence or absence of the amplifier does not affect what is observed.

The essential result of the observations is shown in Fig. 13. We see the following features. The beam profile is smooth and approximately gaussian in the back focal plane of the lens and also at the beam waist.

At a point somewhat beyond the beam minimum the beam begins to show a marked deviation from a smooth profile. This first shows up as a bright spot in the center of the beam. A short distance farther down we encounter a minimum on-axis with a bright ring around it. As we progress farther downstream we see more rings developing in the beam profile.

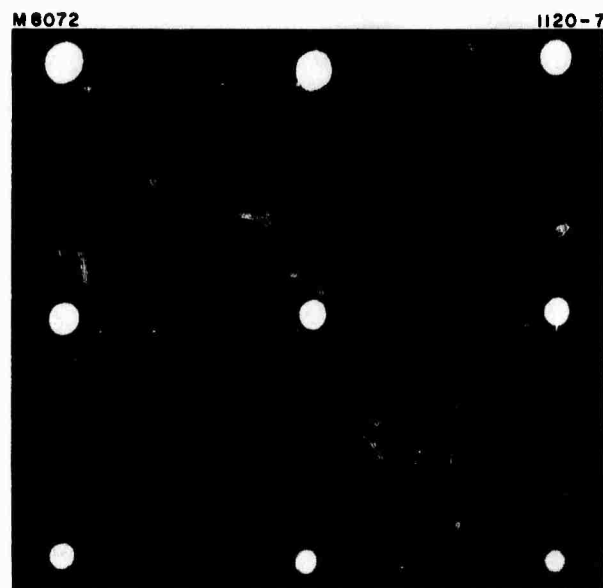
At first we suspected that these peculiar beam profiles might be an artifact of some sort, and attempted to examine more closely the conditions under which they are observed (i. e. , we wanted to find out whether the phenomenon was real).

We found that the same kind of behavior was observed for different focusing lenses and different imaging lenses showing that our observation was not a peculiarity of a particular lens. The pattern of rings, etc. , is reminiscent of what might be expected if spherical aberration were present. To check whether the phenomenon was a property of the lenses or the ruby laser itself, we passed the light from the He-Ne alignment laser through the same setup. A number of regions along the beam were imaged onto the MgO block and photographed. We saw no evidence of rings or other irregularities over the entire range



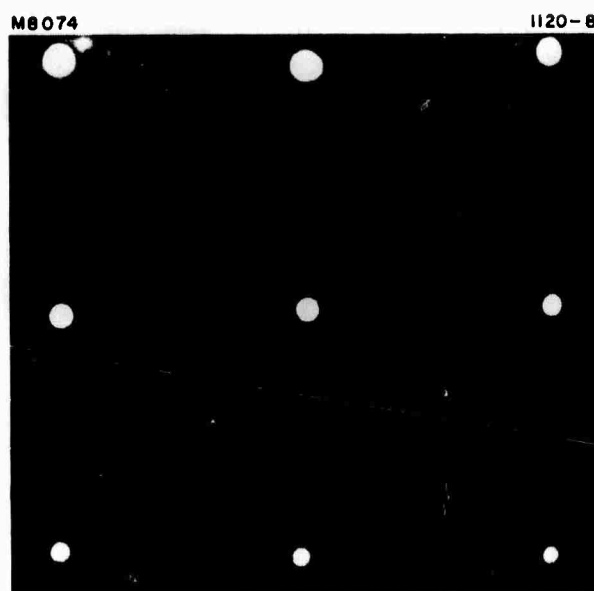
29.0 cm

(a)



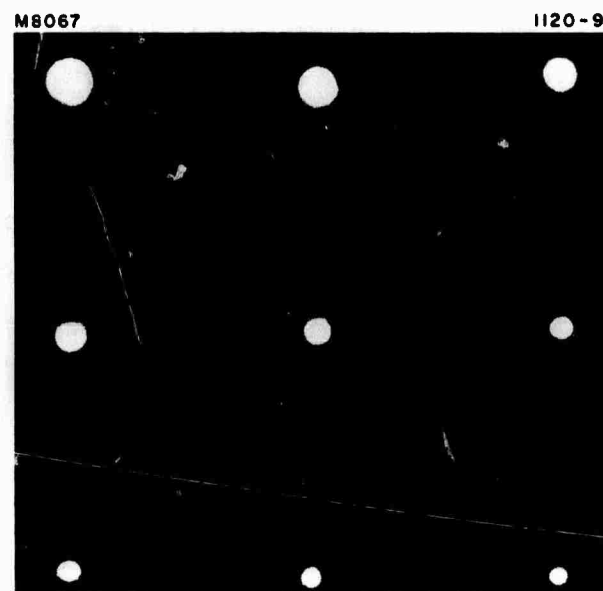
30.0 cm

(b)



31.0 cm

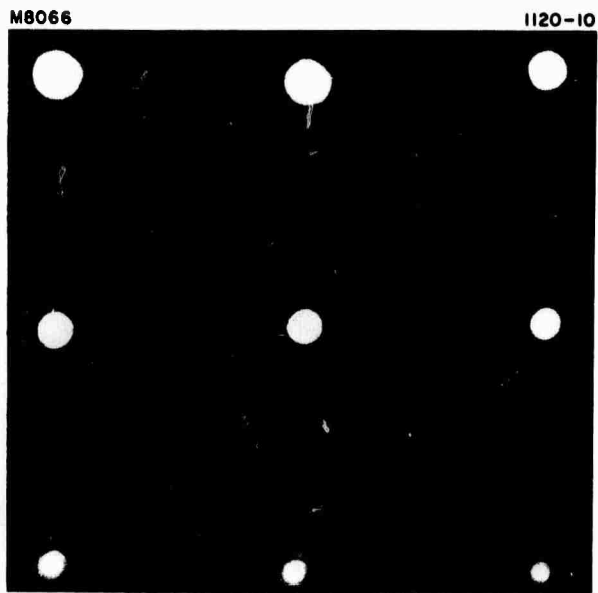
(c)



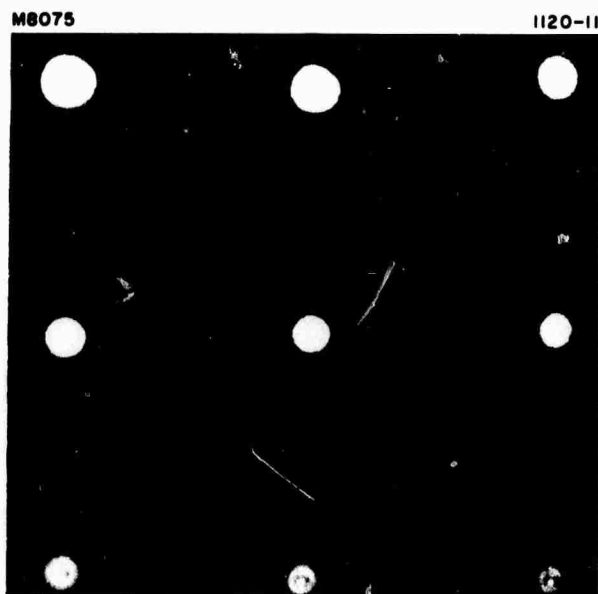
32.0 cm

(d)

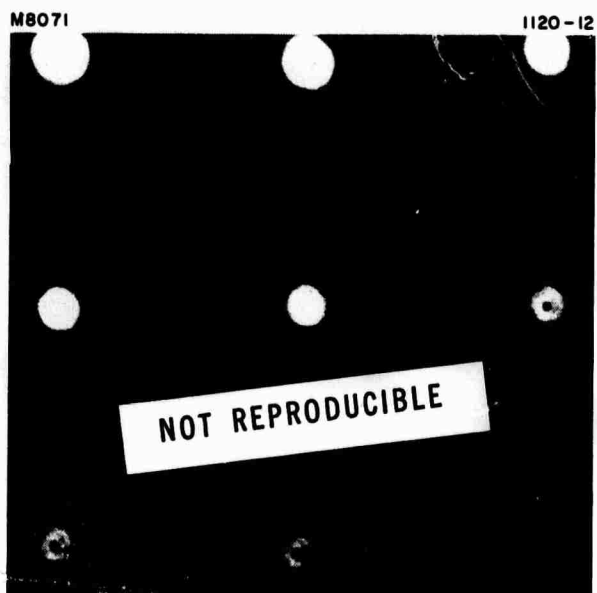
Fig. 13. Beam profile at different distances from 30.5 cm lens. Beam waist is at approximately 31.5 cm.



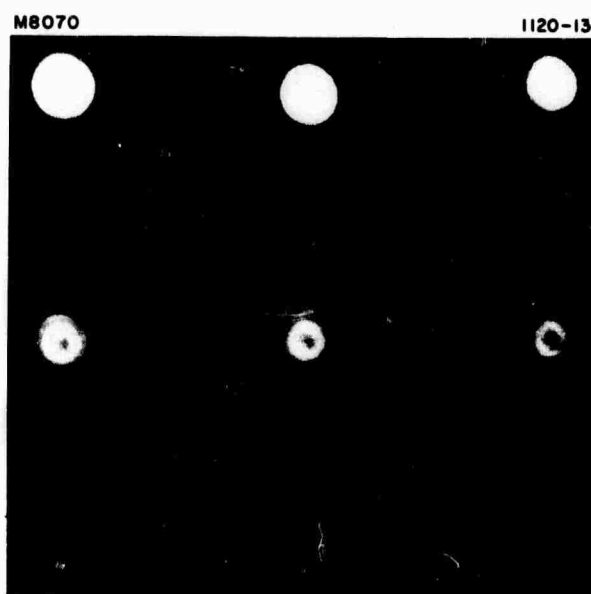
33.0 cm  
(e)



33.5 cm  
(f)

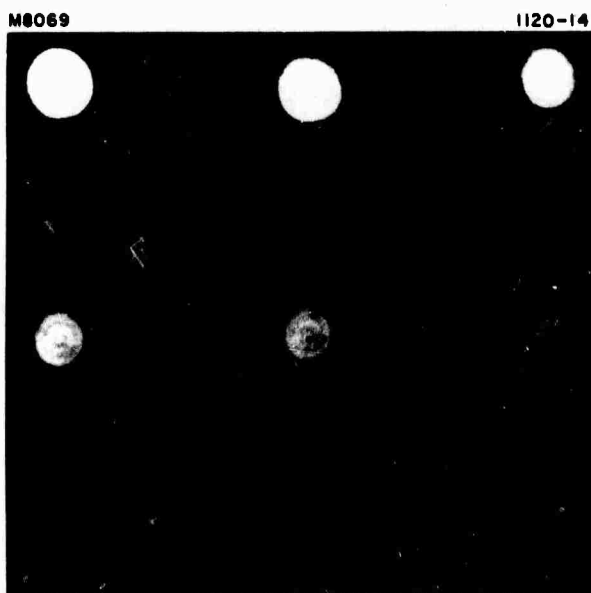


34.0 cm  
(g)



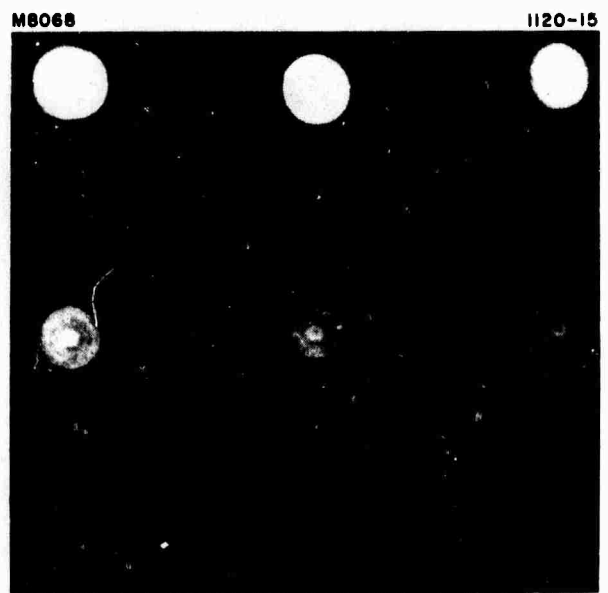
34.5 cm  
(h)

Fig. 13. (Cont'd).



35.0 cm  
(i)

NOT REPRODUCIBLE



35.5 cm  
(j)

Fig. 13. (Cont'd).

of positions on both sides of the beam focus. This led us to conclude that what we observed was a property of the ruby laser itself and not of the lenses.

To reconfirm this conclusion we removed the magnifying lens and placed the MgO block directly in the beam, photographing the spot on the MgO block and choosing the magnification so the spot size in the film plane was the same as in the earlier experiments. We placed the MgO block at a point where a distinct on-axis minimum was observed in the first setup and found no evidence for an on-axis minimum in the photographs. This contradictory evidence led us to believe that perhaps the second lens was responsible. Another possibility was that the graininess of the MgO block was now interfering with our ability to resolve the structure in the beam. In these latter experiments the multiple lens camera was not used because of sensitivity considerations, and because the high magnification required would make it necessary to bring the lens assembly too close to the block, resulting in a geometrical nonequivalence of the camera lenses. Instead a single lens was used to image the spot on the block directly onto the film plane, and in most cases different exposures were taken at the same location in order not to miss the opportunity of detecting any structure.

Further evidence supporting the contention that the structure is a property, at least in part, of the ruby laser itself and not an artifact of the system of observation is as follows.

- The structure is observed with different focusing and imaging lens
- The structure is not simply a propagation phenomenon.

To verify the latter point, we imaged the same plane with lenses of different focal length. Therefore the distance between focusing and imaging lenses is different in each case. The pattern observed is the same in the two experiments, indicating that the imaging lenses are indeed imaging information from the plane of interest. Another similar

experiment was performed in which the distance between the two lenses was kept constant and the MgO block was moved to different positions. Here we were imaging different object planes at different magnifications. Patterns characteristic of the planes of interest when viewed at the same magnification were observed. The pattern changed when the MgO block was moved from one position to the other and the corresponding change was the same as if the new plane was imaged by moving the imaging lens rather than moving the MgO block alone and keeping the lens-to-lens distance fixed.

All these results strongly suggested that the structure that we saw in the photographs was actually a part of the beam. But why couldn't we see it when we placed a diffuser directly in the beam and photographed it at a comparable magnification? Again the question of graininess in the MgO block arises. To check this further we tried putting smoother surfaces into the beam and attempted to make the spot as large as possible. This was accomplished by using the 48.3 cm lens focused onto glossy white paper (exposed Polaroid film). We placed the paper in the beam at the same location where we saw a distinct on-axis minimum in the profile using the two-lens technique. See Fig. 14. Here we see a definite dark spot in the center of the beam photograph although it is not as pronounced as it is in the two-lens technique.

With this result we were convinced that the phenomenon is real and a property of the ruby laser, or perhaps a combined property of the laser and the lenses. We took a few beam profile pictures of the laser output with no lenses in the beam at a number of distances from the laser from 2 to 55 m and saw no evidence of ring structure in the beam profile.

The behavior described above is reminiscent of the description given by Innes and Bloom<sup>12</sup> who discuss beam profiles for focused gaussian beams for different amounts of truncation and spherical aberration. However, the effects that they predict become significant

M 8076

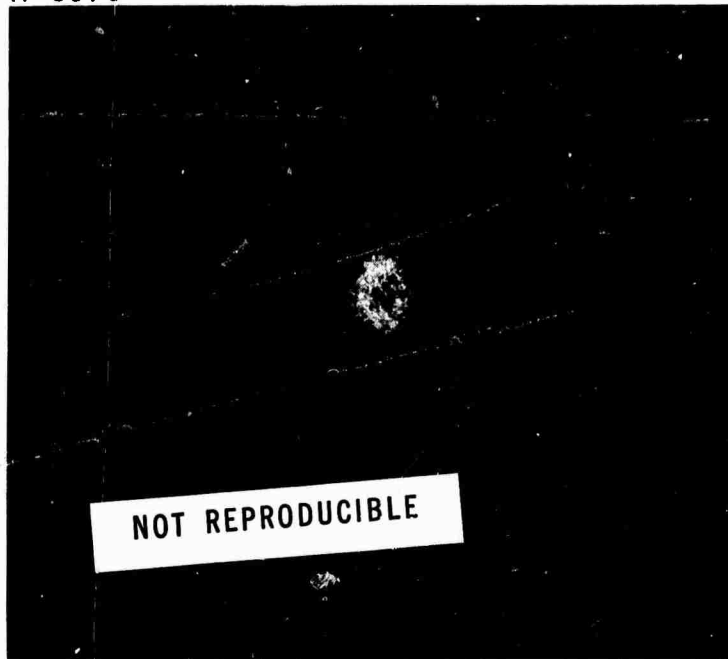


Fig. 14. On-axis minimum in beam profile taken by placing scatterer directly in beam. (63 cm from 48 cm lens).

only for large spherical aberration ( $\lambda/2$ ) and relatively severe truncation of the gaussian beam. Of course, we have no assurance that the phase fronts of our beam are uniform at the output mirror of the oscillator. Nonuniform phase across the beam could certainly give rise to irregularities in the beam profile such as that observed. It is interesting to note that this behavior could well be a general characteristic of all "single mode" solid state lasers. Further pursuit of this phenomenon would certainly be valuable but is probably outside of the realm of the present program.

#### G. PLANS FOR NEXT REPORTING PERIOD

During the next reporting period we will concentrate on the problem of surface damage, with special emphasis on exit surface damage, inasmuch as it has the lowest threshold. Bulk phenomena such as self-focusing will be considered since they may affect the surface damage. Among the experiments we will carry out will be the determination of surface damage threshold as a function of lens-to-sample distance. We will compare the threshold under the conditions where the beam is converging with those where it is diverging, but where the spot size at the exit surface is the same. Such experiments will tell us whether the surface damage threshold is strictly power density dependent or whether it depends on phenomena which are taking place in the bulk of the material. We also will look closely at the exit surface plasma and attempt to study the dynamics of its formation relative to the incident light pulse. We will attempt to find the connection between the plasma and the damage (i. e. , which comes first or which causes which). The interesting results found with the cylindrical lenses will be pursued further; we will try to actually create damage and consequently obtain a measure of the threshold. Also during this period we will examine more closely the streak camera data which we have already taken with

the aim of modifying the theory to include electrostriction so that the fit with the experimental results will be better.

## SECTION II

### THEORETICAL STUDIES ON OPTICAL DAMAGE

#### A. INTRODUCTION

Most of the theoretical effort during the period covered by this report was devoted to an attempt to understand in a fundamental way the heating of electrons in polar crystals by intense optical fields. Several theories have been proposed<sup>13, 14</sup> in which the electrons gain enough energy from the laser radiation to overcome the energy loss due to the radiation of optical phonons and are "heated" to energies exceeding the valence-conduction band energy gap. These hot electrons ionize the lattice, each hot electron producing two slow electrons and a hole, which in turn are heated by the optical field. This results in an avalanche of carrier multiplication which results in a rapid increase in the absorption of laser energy. The absorption of a large energy in a small volume of the crystal is assumed to be the primary cause of the observed damage.

The theories of Zverev, et al., and Wasserman were of the type described above. While appearing reasonable at first glance, they suffer from the weakness of being based on rather heuristic arguments. Both theories predict an avalanche threshold about an order of magnitude greater than that observed in sapphire. Recent experiments at Massachusetts Institute of Technology using CO<sub>2</sub> laser radiation in alkali halide crystals seem to agree with the estimates of Zverev's theory.<sup>16</sup> Hellwarth<sup>15</sup> conducted a study in which he found, on the basis of a more fundamental approach, that electrons could not be heated sufficiently by an optical field in ruby or sapphire to trigger an avalanche process. He suggested some alternate absorption mechanisms.

Because of the apparent controversy concerning the possibility of electron heating and avalanche in an intense optical field in ruby or

sapphire, we have begun an independent study. We have succeeded in deriving a kinetic equation describing the time evolution of the electron momentum (i. e. , lattice momentum) distribution function. The Frölich model of electrons interacting with longitudinal optic phonons in a polar crystal is used as in all the previous studies. The electron-phonon interaction is treated in lowest order perturbation theory. This not a good approximation for ruby or sapphire for which the polar coupling is strong and real polaron effects must be taken into account.<sup>15</sup> However, it is the basis for the work of Zverev<sup>14</sup> and Wasserman<sup>13</sup> and is hoped to be of qualitative value for determining the feasibility of electron heating. In the kinetic theory, which we are developing, the interaction of the electromagnetic field of the laser with the electron is treated exactly to all orders.

Unfortunately, at the time of this report, the research is not complete. The detailed consequences of this kinetic theory are still not understood. Nevertheless, we believe the kinetic equation to be described here offers a fundamental basis to settle the questions of electron heating and work will continue on this problem.

## B. KINETIC EQUATION

We will present a detailed derivation of the kinetic equation for electrons interacting with phonons in an intense ac electric field in another publication. This derivation is based on the Green's function formulation of nonequilibrium quantum statistical mechanics which has been used by the author in several previous studies.<sup>17</sup> Here, we will start from this kinetic equation, carry out some simplifications and discuss its physical content and conditions for validity. Let  $n_p(t) dp_x dp_y dp_z$  be the average number of electrons with lattice momenta in the range  $p_x$  to  $p_x + dp_x$ , etc. Then the equation for the time rate of change for this momentum distribution function is shown to be

$$\begin{aligned}
\frac{dn_p(t)}{dt} = & \frac{-eE_c}{2\pi m^*} \int \frac{d^3k}{k^2} \int_{-\infty}^{\infty} d\omega \int_0^{\infty} dt' \cos\left(\int_{t-t'}^t \frac{d\tau}{\hbar}\right. \\
& \left. \left[ h_{p+k}(\tau) - h_p(\tau) - \omega \right] \right) \\
& \left\{ \left[ 1 + n_{p+k} \left( t - \frac{t'}{2} \right) \right] n_p \left( t - \frac{t'}{2} \right) D_k^<(\omega) \right. \\
& \left. - n_{p+k} \left( t - \frac{t'}{2} \right) \left[ 1 + n_p \left( t - \frac{t'}{2} \right) \right] D_k^>(\omega) \right\} . \quad (4)
\end{aligned}$$

Here,  $E_c$  is a constant with the dimensions of an electric field intensity which measures the strength of the electron-phonon coupling in the Frölich theory

$$E_c = e\omega_{LO} \left( \frac{1}{\epsilon_{\infty}} - \frac{1}{\epsilon_0} \right) \frac{m^*}{\hbar} \quad (5)$$

where  $\omega_{LO}$  is the LO phonon frequency (assumed independent of  $k$ ),  $\epsilon_{\infty}$  and  $\epsilon_0$  are the high frequency and static dielectric constants, respectively, and  $m^*$  is the electron effective mass.

Approximation 1. We emphasize again that this equation is valid only to lowest order in the electron-phonon coupling. The LO phonon spectrum is contained in the functions

$$D_k^<(\omega) = \left[ N_0 \delta(\omega - \omega_{LO}) + (N_0 + 1) \delta(\omega + \omega_{LO}) \right] \quad (6)$$

$$D_k^>(\omega) = e^{\beta\hbar\omega} D_k^<(\omega) , \quad (7)$$

where  $N_0$  is the thermal equilibrium phonon occupation number

$$N_0 = \frac{1}{e^{\beta \hbar \omega_{LO}} + 1} \quad (8)$$

Approximation 2. The phonons are assumed to remain in equilibrium at the lattice temperature  $T = \beta^{-1} k_B^{-1}$  ( $k_B$  = Boltzmann's constant). This approximation will fail once a considerable amount of heating occurs but should be sufficient for the calculation of avalanche thresholds.

The function  $h_p(\tau)$  is the kinetic energy part of the Hamiltonian for an electron in a spatially uniform time-dependent electric field represented by the vector potential  $A(t)$

$$h_p(\tau) = \frac{1}{2m^*} \left( p - \frac{e}{c} A(\tau) \right)^2 \quad (9)$$

The factors

$$\exp \pm i \int_{-t'}^t \frac{d\tau}{\hbar} h_p(\tau)$$

which make up the cosine term in eq. (4) arise from the exact solution of the time-dependent Schrodinger equation in a spatially uniform ac field

$$i\hbar \frac{\partial}{\partial t} \psi_p(t) = h_p(t) \psi_p(t) \quad (10)$$

Thus, the kinetic equation treats the motion of free electrons in the ac field exactly.

Approximation 3. We have assumed a parabolic energy-momentum relation for electrons in the conduction band. This

approximation is easily relaxed to take into account nonparabolicity which is undoubtedly important for electrons excited high in the band.

For the ac field represented by the laser, the vector potential  $A(\tau)$  can be taken to be

$$A(\tau) = \frac{-c E_0}{\omega_0} \sin \omega_0 \tau. \quad (11)$$

Approximation 4. The electromagnetic field is taken to be spatially uniform. This is not bad so long as the magnitude of the classical excursion

$$\underline{d} = \frac{e \underline{E}_0}{m^* \omega_0^2} \quad (12)$$

of an electron in the field is small compared with a wavelength of the actual physical field. This requirement is always well satisfied.

Using this form for the vector potential we obtain

$$\frac{1}{\hbar} \int_{t-t'}^t d\tau \left[ h_{p+k}(\tau) - h_p(\tau) \right] = (\mathcal{E}_{p+k} - \mathcal{E}_p) \frac{t}{\hbar} - \frac{\underline{k} \cdot \underline{d}}{\hbar} \left[ \cos \omega_0 t - \cos \omega_0 (t-t') \right], \quad (13)$$

where  $\underline{d}$  is given by eq. (12) and  $\mathcal{E}_p = p^2/2m^*$ .

Approximation 5. We assume the electron density remains low enough that degeneracy can be neglected, i. e.,  $n_p(t) \ll 1$ . Then the

expression in curly brackets in eq. (4) can be written as

$$\left\{ D^<(\omega) \left[ n_p \left( t - \frac{t'}{2} \right) - n_{p+k}(t-t'/2) e^{\beta \hbar \omega} \right] \right\} \quad (14)$$

where (7) has been used.

Next, we use the well-known Bessel function identity,

$$e^{ia \sin X} = \sum_{\nu} J_{\nu}(a) e^{-i\nu X}, \quad (15)$$

to write

$$\begin{aligned} & \cos \left[ \left( \omega - \epsilon_{p+k} + \epsilon_p \right) \frac{t}{\hbar} + \frac{k \cdot d}{\hbar} \left( \cos \omega_0 t - \cos \omega_0 (t-t') \right) \right] \\ & \text{Re} \left[ e^{i(\omega - \epsilon_{p+k} + \epsilon_p)t/\hbar} \sum_{\mu \nu} J_{\mu} \left( \frac{k \cdot d}{\hbar} \right) J_{\nu} \left( \frac{k \cdot d}{\hbar} \right) e^{i\nu \omega_0 t} \right. \\ & \quad \left. e^{-i\mu \omega_0 (t-t')} e^{i(\nu - \mu)\pi/2} \right] \end{aligned} \quad (16)$$

To consider the periodicity impressed upon the system by the strong ac field, it is useful to write the distribution function as a Fourier series with fundamental frequency  $\omega_0$ , whose coefficients are slowly varying functions of time on the scale of  $\omega_0^{-1}$ .

$$n_p(t) = \sum_n F_n(p, t) e^{-in\omega_0 t}. \quad (17)$$

On substituting eqs. (17), (16), (13), and (14) into eq. (4), we obtain the coupled set of equations for the Fourier coefficients

$$\begin{aligned}
\frac{\partial F_n(p, t)}{\partial t} - i n \omega_0 F_n(p, t) &= \frac{e E_c}{2 \pi m^*} \int \frac{d^3 k}{k^2} \int_{-\infty}^{\infty} d\omega D^<(\omega) \\
\sum_{\mu, m} J_{\mu} \left( \frac{k \cdot d}{\hbar} \right) J_{\mu+m-n} \left( \frac{k \cdot d}{\hbar} \right) &\delta \left( \hbar \omega + \hbar(\mu + m/2) \omega_0 - \varepsilon_{p+k} + \varepsilon_p \right) \\
\left[ F_m(p+k, t) e^{\beta \hbar \omega} - F_m(p, t) \right] &.
\end{aligned} \tag{18}$$

Approximation 6 (Weak Coupling). This is an extremely complicated infinite hierarchy of equations in general. However, if we assume that the electron-phonon interaction as measured by  $E_0$  is weak, then the assumption

$$F_0 \gg F_n \quad \text{for } n \neq 0 \tag{19}$$

is valid. This follows since  $\partial F_n / \partial t \ll n \omega_0 F_n$  for  $n \neq 0$ . Then if we adopt an iterative procedure starting by keeping only the  $m = 0$  term on the right side of eq. (18), we see that  $F_n$  is proportional to  $E_c / n \omega_0$  times  $F_0$  ( $n \neq 0$ ) which we assume to be small. We repeat that this procedure is valid only in the weak coupling limit for the electron-phonon approximation. In fact, the kinetic equation (18) is only valid in this case. This approximation fails for the parameters of ruby and sapphire. We use it mainly because it is the only known procedure for the nonequilibrium polar problem.

Thus, to lowest order in the electron-phonon coupling, the fundamental kinetic equation for the dc component of the electron distribution function is taken to be

$$\begin{aligned}
\frac{\partial F_0(p, t)}{\partial t} &= \frac{e E_c}{2\pi m^*} \int \frac{d^3 k}{k^2} \int_{-\infty}^{\infty} d\omega D^<(\omega) \\
&\sum_{v=-\infty}^{\infty} J_v^2\left(\frac{k \cdot d}{\hbar}\right) \delta(\hbar\omega + v\hbar\omega_0 - \epsilon_{p+k} + \epsilon_p) \\
&\left[ F_0(p+k, t) e^{\beta\hbar\omega} - F_0(p, t) \right] . \quad (20)
\end{aligned}$$

We have not yet succeeded in obtaining a complete solution of this equation. Not the least complication is the involved dependence on the radiation intensity occurring through the Bessel functions  $J_v^2(k \cdot d/\hbar)$ . Examination of the requirements imposed on  $k$  by the delta function shows that values of  $k$  as large as  $\sqrt{2m^*v\omega_0}$  can be important in the integrand. In intensity units then,

$$\left(\frac{k \cdot d}{\hbar}\right)^2 \lesssim v 10^{-9} I ,$$

where  $I$  is in watts/cm<sup>2</sup>. For the laser powers necessary for damage ( $I \sim 10^{10}$  watts/cm<sup>2</sup>), this parameter is large and the Taylor expansions of the Bessel functions cannot be used.

However, to gain some understanding of the consequences of this complicated equation, we have looked at the case of lower intensities for which  $k \cdot d/\hbar \ll 1$  and expanded (20) to terms of order  $(k \cdot d/\hbar)^2$ .

$$\begin{aligned}
\frac{\partial F_o(p, t)}{\partial t} = & \frac{e E_c}{2\pi m^*} \int \frac{d^3 k}{k^2} \int_{-\infty}^{\infty} d\omega D^<(\omega) \\
& \left\{ \left( 1 - \frac{1}{2} \left( \frac{k \cdot d}{\hbar} \right)^2 \right) \delta \left( \hbar\omega - \epsilon_{p+k} + \epsilon_p \right) \right. \\
& + \frac{1}{4} \left( \frac{k \cdot d}{\hbar} \right)^2 \left[ \delta \left( \hbar\omega + \hbar\omega_o - \epsilon_{p+k} + \epsilon_p \right) \right. \\
& \left. \left. + \delta \left( \hbar\omega - \hbar\omega_o - \epsilon_{p+k} + \epsilon_p \right) \right] \right\} \\
& \left[ F_o(p+k, t) e^{\beta \hbar\omega} - F_o(p, t) \right] . \tag{21}
\end{aligned}$$

In this limit the various terms in the equation have a simple interpretation in terms of the transition rates for elementary processes calculated by Fermi's Golden Rule. The first term in curly brackets of order 1 can be shown to produce the difference of the rates for scattering-in and scattering-out of the state  $p$  by emission or absorption of LO phonons. The first term of order  $(k \cdot d/\hbar)^2$  is the correction to these rates for the coherent possibility of absorbing and emitting a photon in this process. The second term of order  $(k \cdot d/\hbar)^2$  produces the difference of the rates of scattering-in and scattering-out of the state  $p$  by either emitting or absorbing a photon and emitting or absorbing an LO phonon. The latter processes are essentially those of electron-phonon Bremstrahlung emission and absorption.

The kinetic equation (20) is not complete for this problem because it does not contain terms which account for the process of impact ionization. We will not try to formulate these terms precisely here,

but rather will discuss their qualitative features. The missing terms consist of a high-energy "sink" or loss term which accounts for those electrons whose energy exceeds the ionization threshold  $\epsilon_1 \gtrsim \epsilon_{\text{gap}}$  and lose their energy by impact ionization collisions with the lattice. There is also a low-energy "source" term which takes into account the two low-energy electrons which appear as a result of the impact ionization processes (i. e., the high-energy electron loses its energy to produce another low-energy electron plus a hole). We may consider that eq. (20) is valid for an intermediate band of energies  $\epsilon_{\text{max}} < \epsilon < \epsilon_1$  where  $\epsilon_{\text{max}}$  is a measure of the maximum energy at which new electrons are created. It appears reasonable to take  $\epsilon_{\text{max}} < \hbar\omega_0$ .

### C. APPROXIMATE CONSIDERATIONS

In an effort to gain some feeling for the predictions of eq. (20) we have taken the case  $k \cdot d < 1$ , which, as we have seen, may not be satisfied by the experiments. However, this case may be useful for understanding the physics involved. As we have seen, the Bessel functions can be expanded in this case as in eq. (21). It is convenient to transform this equation to new variables,  $\epsilon = p^2/2m^*$  and  $\mu$  - the cosine of the angle between the radiation polarization  $\underline{E}_0$  and  $\underline{p}$ .

$$\begin{aligned} \frac{\partial F_0(\epsilon, \mu, t)}{\partial t} = & \frac{e E_c}{p} \int_{-1}^1 d\mu' \int_{-\infty}^{\infty} d\omega D^<(\omega) \\ & \left\{ \frac{1 - (1/2\hbar^2) d^2 (p\mu - p_\omega \mu')^2}{r_\omega} \left[ F(\epsilon + \omega, \mu') e^{\beta \hbar \omega} - F(\epsilon, \mu) \right] \right. \\ & \left. + \frac{d^2}{4\hbar^2} \frac{(p\mu - p_\pm \mu')^2}{r_\pm} \left[ F(\epsilon + \omega \pm \omega_0, \mu') e^{\beta \hbar \omega} - F(\epsilon, \mu) \right] \right\} \quad (22) \end{aligned}$$

where

$$p = \sqrt{2m^* \mathcal{E}}$$

$$p_{\omega} = \sqrt{2m^* (\mathcal{E} + \omega)}$$

$$p_{\pm} = \sqrt{2m^* (\mathcal{E} + \omega \pm \omega_0)} \quad (23)$$

$$r_{\sigma} = \left[ t_{\sigma}^2 - 2t_{\sigma} \mu \mu' + \mu^2 + \mu'^2 - 1 \right]^{1/2} \quad (24)$$

$$t_{\omega} = \frac{1}{2} \left( \frac{p}{p_{\omega}} + \frac{p_{\omega}}{p} \right) ; \quad t_{\pm} = \frac{1}{2} \left( \frac{p}{p_{\pm}} + \frac{p_{\pm}}{p} \right). \quad (25)$$

The last term in eq. (22) is a shorthand notation for the sum of both the + and - indexed quantities.

Next we write  $F_0(\mathcal{E}, \mu) = e^{-\beta X(\mathcal{E}, \mu)}$  and make use of the fact that  $X$  will be a more slowly varying function of  $\mathcal{E}, \mu$  than  $F_0$ . We divide the equation through by  $F_0$ . Differences such as

$$X(\mathcal{E} + \omega \pm \omega_0, \mu') - X(\mathcal{E}, \mu)$$

are Taylor-expanded in the form

$$(\omega \pm \omega_0) X_{\mathcal{E}}(\mathcal{E}, \mu) + (\mu' - \mu) X_{\mu}(\mathcal{E}, \mu)$$

and higher derivative terms dropped. Here  $X_{\mathcal{E}} \equiv \partial X / \partial \mathcal{E}$  and  $X_{\mu} \equiv \partial X / \partial \mu$ . The resulting equation can be written

$$-\beta \frac{\partial X}{\partial t} = \frac{e E_c}{p} \int_{-\infty}^{\infty} d\omega D^<(\omega) \left\{ \left[ A_{\omega}(\mathcal{E}, \mu; X_{\mu}) e^{-\beta \omega (X_{\mathcal{E}} - 1)} - A_{\omega}(\mathcal{E}, \mu; 0) \right] \right. \\ \left. + \frac{d^2 p^2}{\hbar^2} \left[ B_{\pm}(\mathcal{E}, \mu; X_{\mu}) d^{\mp} \beta \omega_0 X_{\mathcal{E}} - B_{\pm}(\mathcal{E}, \mu; 0) \right] \right\}, \quad (26)$$

where we have assumed  $\omega_0 \gg \omega (= \pm \omega_{LO})$  and where we define

$$A_{\omega}(\mathcal{E}, \mu; X_{\mu}) = \int_{-1}^1 d\mu' \frac{e^{-\beta(\mu' - \mu)X_{\mu}}}{r_{\omega}}, \quad (27)$$

$$B_{\pm}(\mathcal{E}, \mu; X_{\mu}) = \int_{-1}^1 d\mu' \frac{\left[ \mu - \left( \frac{p_{\pm}}{p} \right) \mu' \right]^2}{r_{\pm}} e^{-\beta(\mu' - \mu)X_{\mu}}. \quad (28)$$

In the region  $\mathcal{E}_I > \mathcal{E} \gg \omega_0 \gg \omega_{LO}$  it is clear that the parameters  $t_{\sigma}$  defined in eq. (25) all approach unity so that  $A_{-\omega_{LO}} \rightarrow A_{+\omega_{LO}}$  and  $B_{+} \rightarrow B_{-}$ . In this case the integration over  $\omega$  (see eq. (6)) is trivial and the first factor in square brackets on the right side of eq. (22) can be written as

$$N_0 A_{\omega_{LO}}(\mathcal{E}, \mu, X_{\mu}) \left[ \left( e^{-\beta \omega_0 (X_{\mathcal{E}} - 1)} - 1 \right) + e^{\beta \omega_{LO}} \left( e^{\beta \omega_{LO} (X_{\mathcal{E}} - 1)} - 1 \right) \right] \\ + (2N_0 + 1) \left[ A_{\omega_{LO}}(\mathcal{E}, \mu', X_{\mu}) - A_{\omega_{LO}}(\mathcal{E}, \mu, 0) \right] \quad (29)$$

$$\cong N_0 A_{\omega_{LO}}(\mathcal{E}, \mu, X_{\mu}) (\beta \omega_{LO})^2 X_{\mathcal{E}} (X_{\mathcal{E}} - 1) + 2N_0$$

$$\left[ A_{\omega_{LO}}(\mathcal{E}, \mu, X_{\mu}) - A_{\omega_{LO}}(\mathcal{E}, \mu, 0) \right]. \quad (30)$$

In the last member of this equation we have assumed  $\beta\omega_{LO} \ll 1$  and expanded. This is a good approximation for crystals above room temperature. In this limit  $N_o \cong (\beta\omega_{LO})^{-1}$ . In the second term in square brackets on the right side of eq. (22), we note that since  $\beta\omega_o \cong 80$  for the cases of interest, the term with the positive exponential is likely to dominate so we neglect the other terms.

Finally we note that we are expecting exponential growth in the number of carriers during avalanche. Thus we assume that

$$F_o(p, t) = F_o(p) e^{t/\tau}, \quad (31)$$

where  $\tau$  is a characteristic growth time. Then  $\partial F_o / \partial t = F_o / \tau$ . The growth is a result of the high-energy "sink" for  $\mathcal{E} > \mathcal{E}_I$  and the low-energy "source" for  $\mathcal{E} < \omega_o$  which arise from the impact ionization process. These terms do not manifest themselves explicitly in the kinetic equation in the region  $\omega_o < \mathcal{E} < \mathcal{E}_I$  except through the time derivative term. Putting all these assumptions and approximations together leads to the equation

$$\begin{aligned} \frac{(\beta\omega_{LO}) p}{\tau e E_c} &= (\beta\omega_{LO})^2 A_{\omega_{LO}}(\mathcal{E}, \mu, X_\mu) X_{\mathcal{E}}(X_{\mathcal{E}} - 1) \\ &+ 2 \left[ A_{\omega_{LO}}(\mathcal{E}, \mu; X_\mu) - A(\mathcal{E}, \mu, 0) \right] + \frac{2d^2 p^2}{\hbar^2} B_+(\mathcal{E}, \mu; X_\mu) e^{\beta\omega_o X_{\mathcal{E}}}. \end{aligned} \quad (32)$$

We have thus reduced eq. (22), which is an integro-differential-difference equation, to a nonlinear partial differential equation. Unfortunately, we also have not been able to find completely satisfactory analytic approximations to the solution of this equation. It is probably solvable by computer methods, but we have had neither time or support

for this. The boundary conditions for this equation must be determined by examining the physics of the high- and low-energy sink and source terms representing the impact ionization process. This problem is currently under study.

One very approximate conclusion can be obtained from eq. (32). First, we note that for zero radiation intensity and steady state, i. e.,  $d = 0$  and  $\tau = \infty$ , this equation has the solution  $X_e = 1$ ,  $X_\mu = 0$ , corresponding to a Maxwellian distribution at the lattice temperature. Now, in the presence of the radiation the electrons will be "heated" most strongly in the  $\mu = \pm 1$  directions (this follows from the dependence of the field arising as  $k \cdot d$ ). Thus, we might expect the tail of the distribution to be drawn out, i. e.,  $X_e < 1$  in the  $\mu = \pm 1$  directions, but to fall off faster in other directions. This implies  $\beta X_\mu \ll -1$  for  $\mu = +1$ .

From eqs. (27) and (28), it can be shown that for  $\mu \cong 1$  and  $|\beta X_\mu| \gg 1$ ,

$$A_{\omega LO}(\mathcal{E}, 1; X_\mu) = -\gamma - \log \left| \frac{\omega^2 \beta X_\mu}{8\mathcal{E}^2} \right|, \quad (33)$$

where  $\gamma = 0.5772$  (Euler's constant),

$$B_{\pm}(\mathcal{E}, 1, X_\mu) = \frac{2}{(\beta X_\mu)^2}. \quad (34)$$

To a good approximation, an asymptotic relation for  $X_e$  can be obtained from eq. (32).

$$X_e = \frac{1}{\beta \hbar \omega_0} \log \left\{ \frac{(\beta X_\mu)^2}{2I_0} \cdot 10^9 \frac{\omega_0}{\mathcal{E}} \left[ \frac{\tau_{e-ph}(\mathcal{E})}{\tau} + 2(\gamma + \log |2\beta X_\mu|) \right] \right\} \quad (35)$$

where  $\tau_{e-ph}(\mathcal{E}) = \sqrt{2m^* \mathcal{E}} / N_0 E_c$  is the well-known collision time for

electron-polar-optic-phonon collision. This relation is valid as long as the argument of the log is  $\gg 1$ . If  $|\beta X_\mu| \gg 1$ , we see that  $X_e$  is a decreasing function of  $I_0$ , the radiation intensity. In fact, since  $\beta \hbar \omega_0 \cong 80$ ,  $X_e \ll 1$  for any reasonable assignment of parameters. Note that for the term involving the e-folding time  $\tau$  to be important requires  $\tau \ll \tau_{e-ph}$  or  $\tau \ll 10^{-12}$  sec using  $m^* = m_e$  and  $E_c \cong 2 \times 10^2$  e. s. u. for sapphire and  $\mathcal{E} = \hbar \omega_0$ .

If  $\tau \gg \tau_{e-ph}(\mathcal{E})$ , we can neglect the  $\tau$ -dependent term which implies that the steady solution of the kinetic equation (i. e. , eq. (4) with  $\partial F / \partial t = 0$ ) is all we need to consider. In this case, the solution is actually independent of the magnitude of  $E_c$ , as long as it is small enough so that the weak coupling approximation which we have been using is valid. The determination of  $\tau$  as a function of  $I_0$  awaits the completion of the solution satisfying the boundary conditions imposed by the impact ionization process.

This very rough estimate of the behavior of the solution of the kinetic equation makes plausible the following model of the distribution function: The population of electrons is highly nonisotropic, being drawn out into high-energy tails in the ( $\mu = \pm 1$ ) direction of the radiation polarization. These high-energy tails may be sufficient to trigger the strong avalanche of impact ionization events necessary for the Wasserman-Zverev model. However, considerably more analysis of the detailed solution of the kinetic equation is necessary to establish this mode. Note that the average kinetic energy in the distribution will be much lower than the ionization energy  $\mathcal{E}_I$  but there may still be a sufficient number of hot electrons to trigger the avalanche. This is consistent with Hellwarth's observation that the mean kinetic energy of electrons is much lower than the band gap energy.

## REFERENCES

1. J. P. Budin and J. Raffy, Appl. Phys. Letters 9, 291 (1966).
2. G. M. Zverev, T. N. Mikhailova, V. A. Pashkov and N. M. Solov'eva, Pisma Zh. Eksp. Teor. Fiz. 5, 391 (1967); JETP Letters 5, 319 (1967).
3. C. R. Giuliano, D. F. DuBois, R. W. Hellwarth and G. R. Rickel, "Damage Threshold Studies in Laser Crystals," Semiannual Report No. 3, January 1971 — ARPA Order No. 1434.
4. I. M. Winer, Appl. Optics 5, 1437 (1966).
5. E. L. Dawes and J. H. Marburger, Phys. Rev. 179, 862 (1969).
6. D. R. White, J. H. Marburger and E. L. Dawes (to be published).
7. J. H. Marburger, ASTM Symposium on Damage in Laser Materials, Proc. (1971).
8. R. G. Brewer and C. H. Lee, Phys. Rev. Letters 121, 267 (1968).
9. R. Polloni, C. A. Sacchi and O. Svelto, Phys. Rev. Letters 23, 690 (1969); R. Cubeddu, R. Polloni, C. A. Sacchi and O. Svelto, Phys. Rev. A 2, 1955 (1970).
10. E. L. Kerr, "Damage in Laser Glass," A. Glass, A. Guenther, C. Stickley and J. Myers, eds., Amer. Soc. Testing and Materials, Technical Publication 469, p. 23 (1969). See also Ref. 4.
11. M. A. Duguay, J. W. Hansen, and S. L. Shapiro, IEEE J. Quant. Electron. 6, 725 (1970).
12. D. J. Innes and A. L. Bloom, Spectra-Physics Laser Technical Bulletin No. 5, Spectra Physics, Inc. (1966).
13. A. Wasserman, Appl. Phys. Letters 10, 132 (1967).
14. G. M. Zverev, T. N. Mikhailova, V. A. Pashkov and N. M. Solov'eva, Soviet Phys. -JETP 26, 1053 (1968).
15. R. W. Hellwarth, Proceedings of the ASTM Symposium on Laser Damage (June 1970).
16. E. Yablonovitch, private communication.

17. D. F. DuBois, Lectures in Theoretical Physics Vol. IXC, edited by W. E. Brittlin (Gordon and Breach, New York, 1967).